

**FACULTY OF PHYSICS "BABEȘ-BOLYAI
UNIVERSITY" CLUJ-NAPOCA ROMANIA**

**STRUCTURAL, MAGNETIC AND ELECTRONIC
PROPERTIES OF Mn-BASED ALLOYS WITH
APPLICATIONS IN ADVANCED TECHNOLOGIES**

Radu-Cristian Gavrea

Scientific Supervisor:

Prof. Dr. Viorel Pop

Acknowledgments

I am profoundly indebted to all my colleagues and friends who have helped and encouraged me in the elaboration of this thesis. First of all, I would like to express my gratitude to my scientific supervisor Prof. Dr. Viorel Pop who has been a truly dedicated mentor, for his continued support, patience and his invaluable discussions.

I want to express my appreciation to Dr. Diana Benea for the scientific coordination and discussions. I am deeply grateful for her initiatives in the study of new Heusler-type compounds and for her determining role in performing the band structure calculations from this study.

My thanks also go to the members of the doctoral guidance committee: Prof. Dr. Romulus Tetean, Prof. Dr. Daniel Andreica and Prof. Dr. Iosif Grigore Deac for their insights and support during my graduate studies.

I am very thankful to Prof. Dr. Olivier Isnard from Universite Grenoble Alpes and Institute Neel in Grenoble, France, not only for giving me the chance to work in his group but also for his guidance, support, interest, comments and fruitful discussions.

I thank Prof. Dr. Marin Coldea from Universitatea Babes-Bolyai, Cluj-Napoca for his great support and help in the interpretation of some experimental results in Mn-based intermetallic compounds and XPS studies.

Many thanks to my colleague and friend Razvan Hirian for his help, support, and cooperation. I am so grateful for all that I have learned from you.

I am grateful to Prof. Dr. Ionel Chicinas and his research group, from Technical University of Cluj-Napoca for according me the support in performing the structural and microstructural measurements. His group has been always a source of friendships. The SEM images discussed in this thesis would not have been possible without the help of Lucian Barbu-Tudoran from INCDTIM Cluj-Napoca.

I would like to thank to research group from Institute of Physics “Ioan Ursu”, Babes-Bolyai University, for providing a stimulating environment and constant support.

A very special thanks to my family for their support, patient, and encouragement throughout these years. Lastly, but not the least, I would like to thank Alexandra Simon for her understanding, motivation, and love during the past few years.

Table of Contents

Acknowledgments.....	i
List of Tables	vi
List of Figures	vii
Introduction.....	1
Chapter 1.....	3
Magnetism and Magnetic Materials.....	3
1.1 The origin of atomic moments	3
1.2 Classification of Magnetic Materials	3
1.2.1 Diamagnetism	4
1.2.2 Paramagnetism.....	4
1.3. Ordered magnetic materials	4
1.3.1 Ferromagnetism	4
1.3.2 Antiferromagnetism	4
1.3.3 Ferrimagnetism	5
Chapter 2.....	6
Preparation and Characterization techniques.....	6
2.1. Sample preparation	6
2.2 X-Ray Diffraction	6
2.2.1 Takamura's order model.....	7
2.3 Neutron diffraction.....	7
2.4 Differential scanning calorimetry	7
2.5 Energy Dispersive X-ray Spectroscopy	7
2.6 X-ray Photoelectron Spectroscopy	8
2.7 Magnetic measurements.....	8
2.7.1 Extraction and vibrating sample magnetometer	9
2.7.2 Faraday Balance.....	9
2.8 Band structure calculations	9
Chapter 3.....	10
MnAl alloys-A promising RE-free permanent magnetic material.....	10
3.1 General aspects of Mn-Al alloys.....	10
3.2 Structural, electronic and magnetic properties of the $Mn_{54-x}Al_46Ti_x$ ($x = 2; 4$) alloys [19] ...	10
3.2.1 Structural investigations of $Mn_{54-x}Al_46Ti_x$ ($x = 2; 4$) alloys.....	11

3.2.2 Electronic Structure Calculations in $Mn_{54-x}Al_{46}Ti_x$ ($x = 2; 4$) alloys	12
3.2.3. Magnetic experimental investigations of $Mn_{54-x}Al_{46}Ti_x$ ($x = 2; 4$) alloys.....	13
3.3 Conclusions.....	16
Chapter 4.....	17
Structural, Magnetic and Electronic Properties of some Mn-Based Heusler Alloys	17
4.1 General aspects regarding Heusler alloys	17
4.2 Influence of the Cu doping on the electronic structure and magnetic properties of the Mn_2VAl Heusler compound [26].....	18
4.2.1. Structural studies of $Mn_{2-x}Cu_xVAl$ alloys ($x = 0, 0.1, 0.2$ and 0.5)	18
4.2.2 Band structure calculations in $Mn_{2-x}Cu_xVAl$ alloys ($x = 0, 0.1, 0.2$ and 0.5).....	19
4.2.3 Experimental study of magnetic properties in $Mn_{2-x}Cu_xVAl$ intermetallic compound.	19
4.3. Study of the ferrimagnetism and disorder in the half-metallic $Mn_{2-x}Co_xVAl$ Heusler alloy [28 - 29] 21	
4.3.1. Structural studies of $Mn_{2-x}Co_xVAl$ Heusler compounds	21
4.3.2. X-ray photoelectron spectra of $Mn_{2-x}Co_xVAl$ alloys ($x = 0, 0.2, 0.6$ and 1.0)	22
4.3.3. Band structure calculations in $Mn_{2-x}Co_xVAl$ alloys ($x = 0, 0.2, 0.6$ and 1.0).....	23
4.3.4. Magnetic behavior of $Mn_{2-x}Co_xVAl$ Heusler alloys	24
4.4 Half-metallic compensated ferrimagnetism in the Mn-Co-V-Al Heusler alloys [36]	25
4.4.1 Structural characterization of the $Mn_2Co_{1-x}V_xAl$ samples.....	25
4.4.2 Band structure calculations in $Mn_2Co_{1-x}V_xAl$	26
4.4.3 Magnetic behavior of $Mn_2Co_{1-x}V_xAl$ Heusler alloys.....	26
4.5 Conclusions.....	27
5. General conclusions	29
Publications during the Phd period	31
2. Conferences and Summer Schools.....	32
Partial References:	33

Contents of the manuscript of the doctoral thesis

<u>Acknowledgments</u>	i
<u>List of Tables</u>	iv
<u>List of Figures</u>	v
<u>Introduction</u>	1
<u>Chapter 1</u>	3
<u>Magnetism and Magnetic Materials</u>	3
<u>1.1 The origin of atomic moments</u>	3
<u>1.2 Classification of Magnetic Materials</u>	4
<u>1.2.1 Diamagnetism</u>	4
<u>1.2.2 Paramagnetism</u>	5
<u>1.3. Ordered magnetic materials</u>	6
<u>1.3.1 Ferromagnetism</u>	6
<u>1.3.2 Antiferromagnetism</u>	8
<u>1.3.3 Ferrimagnetism</u>	8
<u>Chapter 2</u>	10
<u>Preparation and Characterization techniques</u>	10
<u>2.1. Sample preparation</u>	10
<u>2.2 X-Ray Diffraction</u>	10
<u>2.2.1 Takamura's order model</u>	11
<u>2.3 Neutron diffraction</u>	12
<u>2.4 Differential scanning calorimetry</u>	14
<u>2.5 Energy Dispersive X-ray Spectroscopy</u>	15
<u>2.6 X-ray Photoelectron Spectroscopy</u>	16
<u>2.7 Magnetic measurements</u>	17
<u>2.7.1 Extraction and vibrating sample magnetometer</u>	18
<u>2.7.2 Faraday Balance</u>	19
<u>2.8 Band structure calculations</u>	20
<u>Chapter 3</u>	23
<u>MnAl alloys-A promising RE-free permanent magnetic material</u>	23
<u>3.1 General aspects of Mn-Al alloys</u>	23
<u>3.2 Structural, electronic and magnetic properties of the $Mn_{54-x}Al_4Ti_x$ ($x = 2; 4$) alloys [63] ...</u>	31
<u>3.2.1 Structural investigations of $Mn_{54-x}Al_4Ti_x$ ($x = 2; 4$) alloys</u>	31
<u>3.2.2 Electronic Structure Calculations in $Mn_{54-x}Al_4Ti_x$ ($x = 2; 4$) alloys</u>	34
<u>3.2.3. Magnetic experimental investigations of $Mn_{54-x}Al_4Ti_x$ ($x = 2; 4$) alloys</u>	36

<u>3.3 Conclusions</u>	42
<u>Chapter 4</u>	44
<u>Structural, Magnetic and Electronic Properties of some Mn-Based Heusler Alloys</u>	44
<u>4.1 General aspects regarding Heusler alloys</u>	44
<u>4.2 Influence of the Cu doping on the electronic structure and magnetic properties of the Mn₂VAl Heusler compound [86]</u>	49
<u>4.2.1. Structural studies of Mn_{2-x}Cu_xVAl alloys (x = 0, 0.1, 0.2 and 0.5)</u>	49
<u>4.2.2 Band structure calculations in Mn_{2-x}Cu_xVAl alloys (x = 0, 0.1, 0.2 and 0.5)</u>	53
<u>4.2.3 Experimental study of magnetic properties in Mn_{2-x}Cu_xVAl intermetallic compound</u>	58
<u>4.3. Study of the ferrimagnetism and disorder in the half-metallic Mn_{2-x}Co_xVAl Heusler alloy [94 - 95]</u>	61
<u>4.3.1. Structural studies of Mn_{2-x}Co_xVAl Heusler compounds</u>	62
<u>4.3.2. X-ray photoelectron spectra of Mn_{2-x}Co_xVAl alloys (x = 0, 0.2, 0.6 and 1.0)</u>	68
<u>4.3.3. Band structure calculations in Mn_{2-x}Co_xVAl alloys (x = 0, 0.2, 0.6 and 1.0)</u>	71
<u>4.3.4. Magnetic behavior of Mn_{2-x}Co_xVAl Heusler alloys</u>	74
<u>4.4 Half-metallic compensated ferrimagnetism in the Mn-Co-V-Al Heusler alloys [106]</u>	76
<u>4.4.1 Structural characterization of the Mn₂Co_{1-x}V_xAl samples</u>	77
<u>4.4.2 Band structure calculations in Mn₂Co_{1-x}V_xAl</u>	78
<u>4.4.3 Magnetic behavior of Mn₂Co_{1-x}V_xAl Heusler alloys</u>	83
<u>4.5 Conclusions</u>	85
<u>5. General conclusions</u>	87
<u>Publications during the Phd period</u>	89
<u>Conferences and Summer Schools</u>	90
<u>References:</u>	91

List of Tables

<u>Table 3.1 Values of spontaneous magnetization and coercivity of Mn-Al alloys processed by different techniques.</u>	29
<u>Table 3.2 Magnetic properties (coercivity and remanence) of conventional rare-earth permanent magnets and rare-earth free permanent magnets [61]</u>	29
<u>Table 3.3 The concentrations values of the τ, γ_2 and κ phases and the lattice parameters** of the as-cast and annealed $Mn_{52}Al_{46}Ti_2$ and $Mn_{50}Al_{46}Ti_4$ alloys</u>	33
<u>Table 3.4 Calculated magnetic moments for $Mn_{54}Al_{46}$, $Mn_{52}Al_{46}Ti_2$ and $Mn_{50}Al_{46}Ti_4$ alloys in the AFM configuration.</u>	36
<u>Table 3.5 Spontaneous magnetizations, Curie temperatures, coercive fields and remanent magnetizations of $Mn_{52}Al_{46}Ti_2$ and $Mn_{50}Al_{46}Ti_4$ alloys.</u>	42
<u>Table 4. 1 Crystallographic properties of the as-cast and annealed $Mn_{2-x}Cu_xVAl$ compounds.</u>	50
<u>Table 4.2 Site occupation of the $Mn_{2-x}Cu_xVAl$ ($x = 0.0$ and 0.5) compounds (as-cast and annealed samples).</u>	52
<u>Table 4. 3 Magnetic moments of Mn_2VAl calculated by KKR.</u>	55
<u>Table 4.4 Magnetic moments of $Mn_{1.5}Cu_{0.5}VAl$ calculated by KKR.</u>	57
<u>Table 4.5 The Curie temperatures for $Mn_{2-x}Cu_xVAl$ as-cast and annealed alloys.</u>	59
<u>Table 4.6 Spontaneous magnetization for $Mn_{2-x}Cu_xVAl$ as-cast and annealed alloys.</u>	61
<u>Table 4.7 Structural parameters including S_{B2} and S_{L21} ordering parameters unit cell constant and the site occupation for the as-cast $Mn_{2-x}Co_xVAl$ samples.</u>	64
<u>Table 4.8 The lattice parameters, S_{B2} and S_{L21} ordering parameters and the site occupation for the annealed $Mn_{2-x}Co_xVAl$ samples.</u>	66
<u>Table 4.9 The calculated magnetic moments of the $Mn_{2-x}Co_xVAl$ alloys.</u>	71
<u>Table 4.10 The spontaneous magnetizations and the Curie temperatures of $Mn_{2-x}Co_xVAl$ alloys determined in this work and from literature data.</u>	76
<u>Table 4.11 Calculated magnetic moments for the $Mn_2Co_{1-x}V_xAl$ Heusler alloys with the Hg_2CuTi</u>	79
<u>Table 4.12 Calculated magnetic moments for the $Mn_2Co_{0.5}V_{0.5}Al$, $Mn_{1.92}Co_{0.5}V_{0.58}Al$ and $Mn_{2.07}Co_{0.43}V_{0.5}Al$ Heusler alloys with the Hg_2CuTi structure type.</u>	80
<u>Table 4.13 The spontaneous magnetization and the Curie temperatures of the $Mn_2Co_{1-x}V_xAl$ Heusler alloys determined by magnetic measurements and from literature data.</u>	84

List of Figures

<u>Figure 1.1</u> The temperature dependence of the spontaneous magnetization M_s ($T < T_c$) and of reciprocal magnetic susceptibility $1/\chi$ ($T > T_c$) for a ferromagnetic system.....	7
<u>Figure 1.2</u> The hysteresis loop.....	7
<u>Figure 1.3</u> The temperature dependence of the spontaneous magnetization M_s ($T < T_c$) (three cases are presented) for a ferrimagnetic system consisting of two A and B sublattices [2]	9
<u>Figure 2.1</u> Schematic diagram of interactions of neutrons and X-ray with the matter	13
<u>Figure 2.2</u> Schematic diagram of D1B powder diffractometer [8]	14
<u>Figure 2.3</u> DSC schematic diagram (a) and experimental setup (b).	15
<u>Figure 2.4</u> Description of Energy Dispersive X-ray Spectroscopy principle [10].	16
<u>Figure 2.5</u> The schematic representation of the XPS experiment	17
<u>Figure 2.6</u> Schematic diagram of an extraction or VSM magnetometer	19
<u>Figure 2.7</u> Schematic diagram of the Faraday Balance.....	20
<u>Figure 3.1</u> Al-Mn binary phase diagram [28].....	24
<u>Figure 3.2</u> The ordered $L1_0$ τ -phase structure.....	25
<u>Figure 3.3</u> Phase transformation proposed by Broek et. al. [37] with intermediate ordered orthorhombic phase (B19) denoted by ϵ'	26
<u>Figure 3.4</u> XRD patterns of the as-cast and annealed $Mn_{52}Al_{46}Ti_2$ and $Mn_{50}Al_{46}Ti_4$ samples. The peaks corresponding to the τ and γ_2 phases are indicated. For clarity the diffraction patterns have been shifted vertically.....	32
<u>Figure 3.5</u> The 211 peaks of τ phase for the as-cast (a), TT 470°C 6h (b) and TT 1050°C 1h (c) samples of $Mn_{54-x}Al_{46}Ti_x$	34
<u>Figure 3.6</u> Total energy calculations for the $(Mn_{50-x}Ti_x)^{1a,1c}(Al_{46}Mn_xTi_{4-x})^{2e}$ system.	35
<u>Figure 3.7</u> The temperature dependence of magnetizations for $Mn_{52}Al_{46}Ti_2$ alloys measured in 0.1 T magnetic field. In the inset is shown the temperature dependence of the differential magnetization for the sample annealed at 470°C for 6h.....	37

<u>Figure 3.8 The temperature dependence of the magnetizations for the Mn₅₀Al₄₆Ti₄ alloys measured in 0.1 T magnetic field. In the inset is shown the temperature dependence of the differential magnetization for the as-cast sample.</u>	38
<u>Figure 3. 9 The $M^2(T)$ plot for Mn₅₀Al₄₆Ti₄ as-cast sample.</u>	38
<u>Figure 3. 10 The temperature dependence of the magnetizations for the Mn₅₂Al₄₆Ti₂ and Mn₅₀Al₄₆Ti₄ (inset) alloys measured in 7 T magnetic field.</u>	39
<u>Figure 3. 11 The virgin magnetization curve and the demagnetization curves for the as-cast and annealed Mn₅₂Al₄₆Ti₂ samples at 4 K. In the inset is shown the region around the origin of the plot.</u>	40
<u>Figure 3. 12 The virgin magnetization curve and the demagnetization curves for the as-cast and annealed Mn₅₀Al₄₆Ti₄ samples at 4 K. In the inset is shown the region around the origin of the plot.</u>	41
<u>Figure 4.1 X₂YZ L₂₁-type crystal structure of Heusler alloys (a) and inverse Heusler (b).</u>	45
<u>Figure 4.2 The Slater-Pauling curve for transition metals and some alloys [66].</u>	46
<u>Figure 4.3 X-ray diffraction patterns of the Mn_{2-x}Cu_xVAI as-cast samples. The data are normalized to the intensity of the (220) reflection. XRD patterns are zoomed 6 times on Y scale for 2θ from 20 to 35 deg, left figure.</u>	49
<u>Figure 4.4 DSC curves for the Mn₂VAI (a) and Mn_{1.5}Cu_{0.5}VAI (b) samples.</u>	51
<u>Figure 4. 5 X-ray diffraction patterns of the Mn_{1.5}Cu_{0.5}VAI TT 800 °C 72 h and Mn₂VAI TT 700 °C 72 h. The patterns are normalized to the intensity of the (220) reflections. XRD patterns are zoomed 6 times on Y scale, for 2θ from 20 to 35 deg, left figure.</u>	52
<u>Figure 4.6 The spin-resolved DOS for the 'ideal' (a) and 'disordered' (b) Mn₂VAI. The origin of the energy scale is the Fermi level.</u>	54
<u>Figure 4.7 The spin- and element-resolved DOS of the 'ideal' (a) and 'disordered'(b) Mn_{1.5}Cu_{0.5}VAI. The origin of the energy scale is the Fermi level.</u>	56
<u>Figure 4.8 The temperature dependence of the magnetization for Mn_{2-x}Cu_xVAI as-cast (a) and annealed alloys (b) measured in low magnetic field.</u>	59
<u>Figure 4.9 Magnetization curves for Mn_{2-x}Cu_xVAI as-cast (a) and annealed (b) alloys measured at 2K.</u>	60
<u>Figure 4.10 EDX spectrum of the as-cast MnCoVAI alloy.</u>	62
<u>Figure 4.11 Room temperature X-ray diffraction pattern of the as-cast Mn_{2-x}Co_xVAI samples. The data are normalized to the intensity of the (220) reflection. The</u>	

<u>superstructure peaks are zoomed 6 times on Y scale for 2θ from 25 to 32 deg., left figure.</u>	63
<u>.....</u>	63
<u>Figure 4.12 DSC curve for the MnCoVAI samples.....</u>	65
<u>Figure 4.13. X-ray diffraction pattern (details of (111) and (200) peaks) of Mn_{2-x}Co_xVAI annealed samples.....</u>	65
<u>Figure 4.14 The lattice constant vs. the Co content in the Mn_{2-x}Co_xVAI Heusler compounds.</u>	67
<u>.....</u>	67
<u>Figure 4.15 Room temperature neutron diffraction pattern for the as-cast Mn_{2-x}Co_xVAI sample (x = 0).....</u>	68
<u>Figure 4.16 XPS spectra of Mn 3s in Mn₂VAI alloy.....</u>	69
<u>Figure 4.17 XPS spectra of V 3s in Mn₂VAI alloy.....</u>	69
<u>Figure 4.18. XPS spectra of Mn 3s core level in MnCoVAI alloy.....</u>	70
<u>Figure 4.19 The spin-resolved DOS for Mn_{2-x}Co_xVAI alloys. The origin of the energy scale is the Fermi level. For x = 0, 0.2 and 0.6, the experimental lattice constant has been used. For x = 1, the calculations have been done with an increased lattice constant (5.86 Å) compared with the experimental one (5.80 Å).....</u>	72
<u>Figure 4.20 The comparison between the experimental and theoretical valence bands for the Mn_{2-x}Co_xVAI alloys, x=0 (a) and x=1 (b).....</u>	73
<u>Figure 4.21 Magnetization curves of Mn_{2-x}Co_xVAI alloys at 2K in magnetic field up to 10 T, annealed at 700 °C (x=0) and 800 °C (x=0.2, 0.6 and 1).....</u>	74
<u>Figure 4.22 Temperature dependences of the magnetization for Mn_{2-x}Co_xVAI alloys annealed at 700 °C (x=0) and 800 °C (x=0.2, 0.6 and 1) measured in low magnetic fields,</u>	75
<u>Figure 4.23 The XRD patterns for Mn₂Co_{1-x}V_xAl (x = 0, 0.1, 0.3 and 0.5) Heusler alloys..</u>	78
<u>Figure 4.24 The density of states of the Mn₂CoAl Heusler alloy. The origin of the energy scale is the Fermi level,</u>	81
<u>Figure 4.25 Density of states for Mn₂Co_{0.5}V_{0.5}Al Heusler alloys for (V_{0.5}Co_{0.5})^{4a}Mn^{4b}Mn^{4c}Al^{4d} (a) and (Mn_{0.5}Co_{0.5})^{4a}(Mn_{0.5}V_{0.5})^{4b}Mn^{4c}Al^{4d} (b) sites occupation,</u>	82
<u>Figure 4.26 Magnetization isotherms at 2 K in a magnetic field up to 10 T for Mn₂Co_{1-x}V_xAl alloys.....</u>	83

Introduction

Nowadays, the interest in developing new materials has dramatically increased due to promising properties that makes these new materials potentially useful for many future commercial applications. The modern computer simulation methods have led to a development of these new materials faster than ever before.

The permanent magnets represent a class of materials that are indispensable for a wide range of application like electric motors, generators, loudspeakers, laptops, etc. Most of the permanent magnets contain strategic rare-earth elements. Recently, the world's largest provider of rare-earth elements (China) has restricted export. This has led to a global crisis and of course an exaggerated increase in the prices of these RE elements. Therefore, the development of alternative magnetic materials like RE-free permanent magnets became inevitable. An interesting candidate with promising high magnetic properties studied in this work is Mn-Al alloy.

Another class of ferromagnetic materials which are intensively studied for spintronic applications (magnetic field sensors, non-volatile data storage devices, magnetic random access memories etc.) are Heusler alloys. In standard electronic devices, the information is carried by the electron charge, while in spintronic devices the spin is in charge to carries the information. Most of Heusler alloys are half-metallic ferromagnets.

The novelty of these half-metallic Heusler alloys is provided by the two spin bands which shows simultaneously a totally distinct behavior: (i) the majority spin channel is metallic and (ii) insulating/semiconducting characteristics due to the band gap around the Fermi level in the minority channel. Consequently, at Fermi level, the material could be spin polarized to 100%, making them ideal for spintronic applications.

The aim of the present work was to study two different classes of materials: Rare-Earth Free Permanent Magnets (τ -MnAl phase) and Heusler alloys. This study was focused on both theoretical and experimental investigations in order to evidence their structural, magnetic and electronic properties.

The thesis is divided into 5 main chapters. First chapter is planned as an overview of magnetic materials. It describes the essential notions required to discuss the following chapters in detail. This section of the thesis is presented to define the origin of magnetism in matter and also how magnetic interactions establish material properties.

The second chapter describes in detail the theoretical and experimental techniques including sample preparation, characterization methods, apparatus used for experiment as well as its measurement principles.

Chapter three consists two main subchapters. The first part of the chapter summarizes the actual context of RE-free permanent magnets and provides an overview of Mn-Al alloys as a promising RE-free permanent magnet taking into account the different approaches from the literature. The second part of the chapter presents in detail our original results on the structural, electronic and magnetic properties of the $\text{Mn}_{54-x}\text{Al}_{46}\text{Ti}_x$ ($x = 2; 4$) alloys. This subchapter ends with the main conclusions following our research on Mn-Al alloys.

Chapter four is divided into five sections. First section provides a short background about the structure and relevant properties of the Heusler alloys, while in the next three sections are presented our findings on the structural, electronic and magnetic properties of the investigated

Heusler alloys. The last section presents the main conclusions about all three Heusler systems investigated in this work.

In the last chapter the general conclusions are described based on the results of studies contained in this thesis.

The experimental investigations included in the current thesis were conducted within several research centers from Romania or abroad: Ioan Ursu Institute of Physics at the Faculty of Physics, Babes-Bolyai University, Cluj-Napoca, Romania; CNRS, Institute Neel, Grenoble, France; ILL Grenoble; INCDTIM, Cluj-Napoca, Romania and Technical University of Cluj-Napoca, Romania.

Chapter 1.

Magnetism and Magnetic Materials

1.1 The origin of atomic moments

The magnetism of substances is controlled by the atomic magnetic moments and the interaction between them. The magnetic moments of atoms arise from the total angular momentum of the electrons. The nucleons (protons and neutrons) carry a small magnetic moment compared to that of electrons, the nuclear part being about three orders of magnitude smaller. The values of \vec{L} and \vec{S} of the total atomic orbital momentum and of the total atomic spin momentum respectively, are coupled through the spin-orbit interactions and defines the value of total kinetic momentum of atom \vec{J} :

$$\vec{J} = \vec{L} + \vec{S} \quad (1.1)$$

At the total atomic momentum \vec{J} , we can associate an atomic magnetic moment $\vec{\mu}$:

$$\vec{\mu} = -g\mu_B\vec{J} \quad (1.2)$$

where μ_B is the Bohr magneton and g is the Landé factor.

1.2 Classification of Magnetic Materials

Magnetic behavior of substances may be divided into three main classes which are diamagnetism, paramagnetism and ordered magnetic behavior (the most known being ferromagnetism, antiferromagnetism and ferrimagnetism).

1.2.1 Diamagnetism

Diamagnetism is a very weak contribution to the material's response to an applied magnetic field exhibited by all substances. It arises from influence induced by an applied field in the electron shells. There is a change of the orbital angular momentum of the electrons due to applied magnetic field which will develop a negative magnetic moment relatively to the applied field. The magnetic susceptibility of diamagnetic materials is negative and has no temperature dependence [1].

1.2.2 Paramagnetism

The paramagnetic substances are weakly attracted by the magnetic field. This behavior occurs due to the atomic magnetic moments given by the unpaired electrons from the incomplete electronic orbitals. The atomic magnetic moments of paramagnetic substances do not interact with each other. In the presence of an externally applied magnetic field, in order to minimize the Zeeman energy of a magnetic moment in the magnetic field, the magnetic moments will partially align on the direction of the magnetic field. In this case, we have a positive magnetization and positive susceptibility.

1.3. Ordered magnetic materials

1.3.1 Ferromagnetism

Ferromagnetic materials exhibit a spontaneous magnetization even in the absence of a magnetic field due to the strong interactions, exchange interactions between atomic magnetic moments, which imposes a positive coupling of magnetic dipoles and consequently to the parallel alignment of magnetic moments.

1.3.2 Antiferromagnetism

In antiferromagnetic materials, the exchange interaction between neighboring atoms are negative and leads to an anti-parallel alignment of the atomic magnetic moments, thus having a spontaneous magnetization equal to zero.

1.3.3 Ferrimagnetism

The exchange interactions in ferrimagnet materials are negative, as for the antiferromagnets, but the different sublattice magnetizations are unequal, which leads to a non-zero spontaneous magnetization similar to the ferromagnetic materials. Analogous to ferromagnets, the spontaneous magnetization of ferrimagnets vanishes for temperature higher than Curie temperature.

Chapter 2.

Preparation and Characterization techniques

This chapter presents all the experimental and theoretical details concerning the samples preparation and structural, magnetic and electronic investigations. The temperature is given in two units: (i) Celsius degree for aspects concerning sample preparation and heat treatments and (ii) Kelvin temperature scale were used to discuss magnetic behavior.

2.1. Sample preparation

Polycrystalline samples were prepared by induction melting in a cold copper crucible under argon atmosphere in order to avoid contamination. High purity starting materials (> 99.99%) were weighted in exact stoichiometric proportions and melted together. In order to ensure a good homogeneity, the samples were melted several times in the same atmosphere. The weight loss of the final samples was found to be less than 1%. After melting, the samples were wrapped in tantalum foil, sealed in quartz tubes and annealed at different temperature and time in an inert Ar atmosphere followed by quenching in water.

2.2 X-Ray Diffraction

X-ray diffraction (XRD) is a nondestructive technique for characterizing crystalline materials and provides information on crystal structure, crystallographic phases, preferred crystal orientation (texture) and other structural and microstructural parameters, such as grain size, strain and crystal defects.

2.2.1 Takamura's order model

The Takamura's model was employed [2] to investigate the substitutional disorder in our X_2YZ Heusler alloys. In this model, two types of ordering parameters (X-YZ and Y-Z) have been defined to describe the intermixing between the atomic positions.

2.3 Neutron diffraction

Neutron diffraction is a method to investigate the crystal and magnetic structure. This technique may offer many advantages than X-ray diffraction, due to the complementary information that can be obtained, considering the scattering properties of neutrons versus X-rays [2-3]. In particular, an important advantage of this method is the possibility of determining the ordering of magnetic structures of the investigated sample.

2.4 Differential scanning calorimetry

Differential scanning calorimetry (DSC) was employed to study the structural transformations and phase transitions in the 50 – 1000 °C temperature range under Ar atmosphere with a temperature ramp rate of 20 °C/min.

2.5 Energy Dispersive X-ray Spectroscopy

In order to check the stoichiometry of our samples, we employed Energy Dispersive X-ray Spectroscopy (EDS or EDX) measurements. EDX is an X-ray microanalytical technique that is used to provide information about chemical composition of a sample for elements with atomic number $Z > 3$.

2.65 X-ray Photoelectron Spectroscopy

X-ray Photoelectron Spectroscopy is known as XPS or ESCA ((Electron Spectroscopy for Chemical Analysis) was used to investigate the electronic structure of materials studied in this work. X-ray photoelectron spectroscopy (XPS) is based on the photoelectric effect. When an X-ray beam is directed to the sample surface, the incident photons are absorbed into the sample. The energy of photons ($h\nu$) is transferred to the core electrons, which will be excited and emitted on the sample surface if $h\nu$ is large enough. The emitted electron with the kinetic energy of E_k is called photoelectron.

2.7 Magnetic measurements

Magnetic measurements were made with three magnetometers: Faraday balance, extraction magnetometer and vibrating sample magnetometer. The spontaneous magnetization values M_s were determined from the linear extrapolation of magnetization according to the following equation:

$$M = M_s + \chi_0 H \quad (2.2)$$

where χ_0 is the magnetic susceptibility independent of the magnetic field.

In molecular field approximation, at temperatures close to the Curie temperatures, the spontaneous magnetization can be described by the relation:

$$(M/M_s)^2 = \frac{10}{3} \frac{J+1^2}{J^2+(J+1)^2} \left(1 - \frac{T}{T_c}\right) \quad (2.3)$$

where J is total kinetic momentum of atom. According to the equation 2.9, $M^2(T)$ plot is linear and will intersect the temperature axis at $T = T_c$ [5]. Therefore, the Curie temperatures T_c were determined in the molecular field approximation from the M^2 vs. T plot.

2.7.1 Extraction and vibrating sample magnetometer

The magnetic properties (such as coercive field, remanence or spontaneous magnetization) of the investigated samples were measured by using the extraction magnetometer [6] placed at Institute Néel, Grenoble, France and the vibrating sample magnetometer (VSM) from Ioan Ursu Institute of Physics, Babes-Bolyai University, Cluj-Napoca, Romania. The measuring principle of magnetometers is based on the electromagnetic induction phenomenon.

2.7.2 Faraday Balance

This method was used in order to measure the thermal changes (transitions) of the sample magnetization while the temperature is varying. Therefore, it can be determined the Curie temperature of ferromagnetic or ferrimagnetic materials, compensation temperatures or to detect different magnetic phases of the investigated sample.

2.8 Band structure calculations

Theoretical investigations of the electronic and magnetic properties of our compounds have been performed using the Munich SPR-KKR package [7]. The electronic structure of the investigated samples in the ferromagnetic or ferrimagnetic state was calculated by means of the spin-polarized relativistic Korringa-Kohn-Rostocker (KKR) method [7–9].

SPRKKR method provides a very flexible framework to deal with a wide range of systems and properties in electronic structure theory.

Chapter 3.

MnAl alloys-A promising RE-free permanent magnetic material

3.1 General aspects of Mn-Al alloys

As potential rare-earth-free permanent magnets, the Mn-Al alloys have been intensively investigated both experimentally and theoretically in order to improve their intrinsic magnetic properties [10–14]. In Al-Mn phase diagram, Figure 3. 1, in the composition range of 50-60 atomic percent manganese, a metastable ferromagnetic τ -phase with remarkable magnetic properties can be observed [16]. Therefore, the ferromagnetic τ -phase of Mn-Al alloy became an interesting candidate for the permanent magnet applications with important potential due to its appreciable intrinsic properties. Also, this system has a huge economic advantage due to the availability of component elements. The previous studies reported a value of 0.75 T for spontaneous magnetization, an anisotropy constant K_1 of 1.7 MJ/m³, a Curie temperature of 650 K and an estimated maximum energy product at room temperature of 112 kJ/m³ [13, 16-17], being higher than those of conventional RE-free permanent magnets like ferrites or alnico. The aim of our work was to improve the magnetic properties (through the addition of the third element) by reducing the antiferromagnetic coupling between the neighboring Mn-Mn atoms from the adjacent layers.

3.2 Structural, electronic and magnetic properties of the Mn_{54-x}Al₄₆Ti_x (x = 2; 4) alloys [19]

The structural, electronic and magnetic behavior of the as-cast and annealed Mn₅₂Al₄₆Ti₂ and Mn₅₀Al₄₆Ti₄ alloys have been studied through electronic band structure calculations, X-ray diffraction and magnetic measurements in the temperature range 4–850 K and magnetic field up to 7 T.

3.2.1 Structural investigations of $Mn_{54-x}Al_{46}Ti_x$ ($x = 2; 4$) alloys

Because the highest τ phase content was obtained for the parent $Mn_{54}Al_{46}$ alloy annealed at 470°C for 6h [20], the $Mn_{52}Al_{46}Ti_2$ and $Mn_{50}Al_{46}Ti_4$ alloys were annealed under the same conditions. The XRD patterns of the as-cast and annealed $Mn_{52}Al_{46}Ti_2$ and $Mn_{50}Al_{46}Ti_4$ alloys are shown in 3.4 a) and b), respectively.

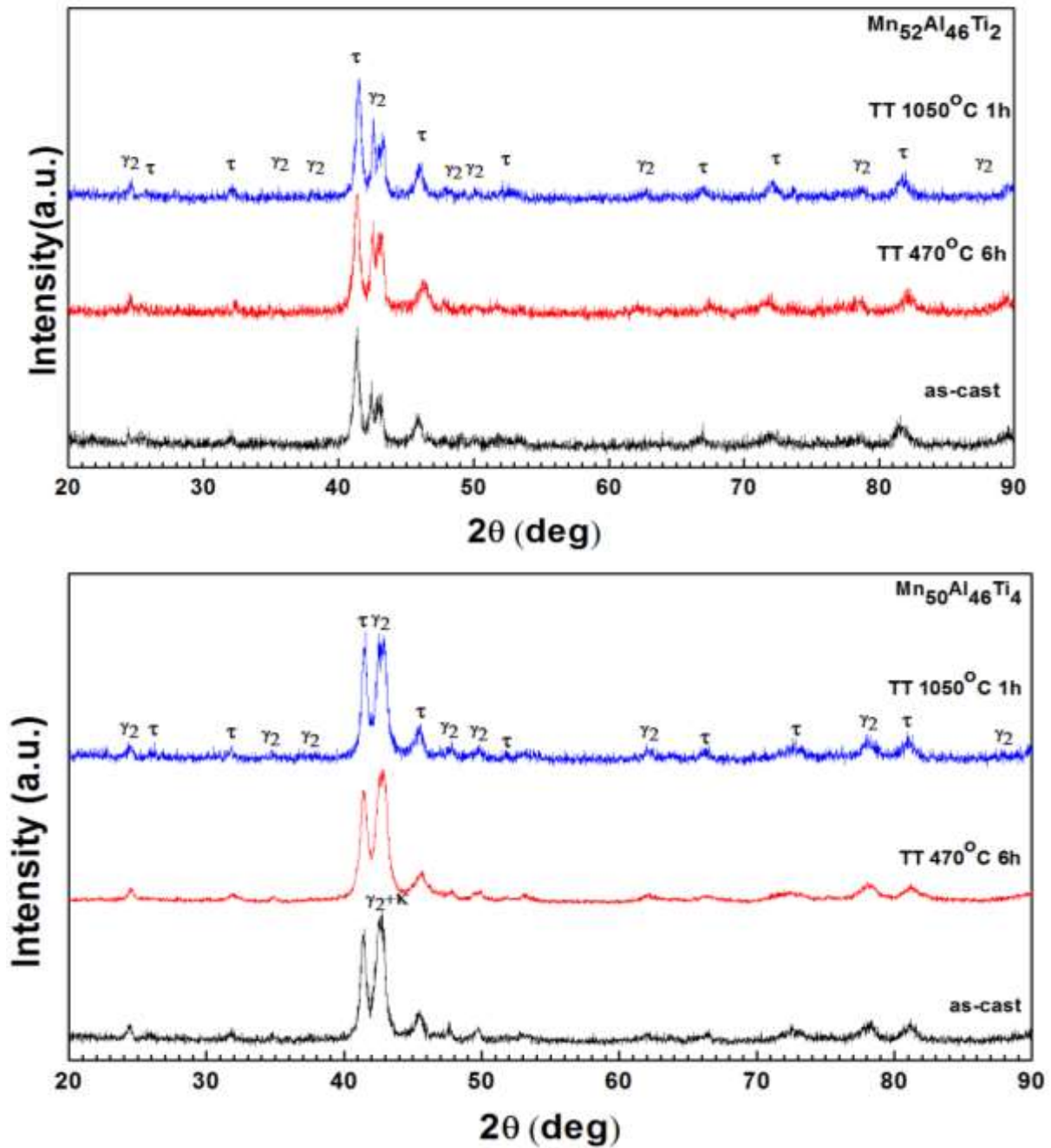


Figure 3.1 XRD patterns of the as-cast and annealed $Mn_{52}Al_{46}Ti_2$ and $Mn_{50}Al_{46}Ti_4$ samples. The peaks corresponding to the τ and γ_2 phases are indicated. For clarity the diffraction patterns have been shifted vertically.

It can be seen that both as-cast and annealed alloys are phase mixtures. All the analyzed samples contain τ and γ_2 phases, however the $\text{Mn}_{50}\text{Al}_{46}\text{Ti}_4$ alloys contain an additional κ phase (CsCl-structure type).

3.2.2 Electronic Structure Calculations in $\text{Mn}_{54-x}\text{Al}_{46}\text{Ti}_x$ ($x = 2; 4$) alloys

The SPRKKR calculations have been performed for $\text{Mn}_{54}\text{Al}_{46}$, $\text{Mn}_{52}\text{Al}_{46}\text{Ti}_2$ and $\text{Mn}_{50}\text{Al}_{46}\text{Ti}_4$ using the experimental determined lattice parameters. The crystal structure considered in the electronic structure calculations is P4/mmm (space group no. 123), with the 1a, 1c and 2e sites occupied [21-22]. In agreement with the previous reports [21, 23], we considered that the Mn magnetic moments in the Mn plane (Mn^{1a} and Mn^{1c} sites) are coupled antiparallel with the Mn magnetic moments in the Al plane (Mn^{2e} site). Total energy calculations have been performed in order to check the preferential occupation of Ti for the 1a, 1c or 2e crystal sites. The antiferromagnetic coupling between Mn moments on 1a and 1c sites and the magnetic moments on 2e site is the stable configuration (Figure. 3.6). The smallest total energy of $\text{Mn}_{52}\text{Al}_{46}\text{Ti}_2$ and $\text{Mn}_{50}\text{Al}_{46}\text{Ti}_4$ alloys was obtained for Ti atoms sitting on the 2e sites.

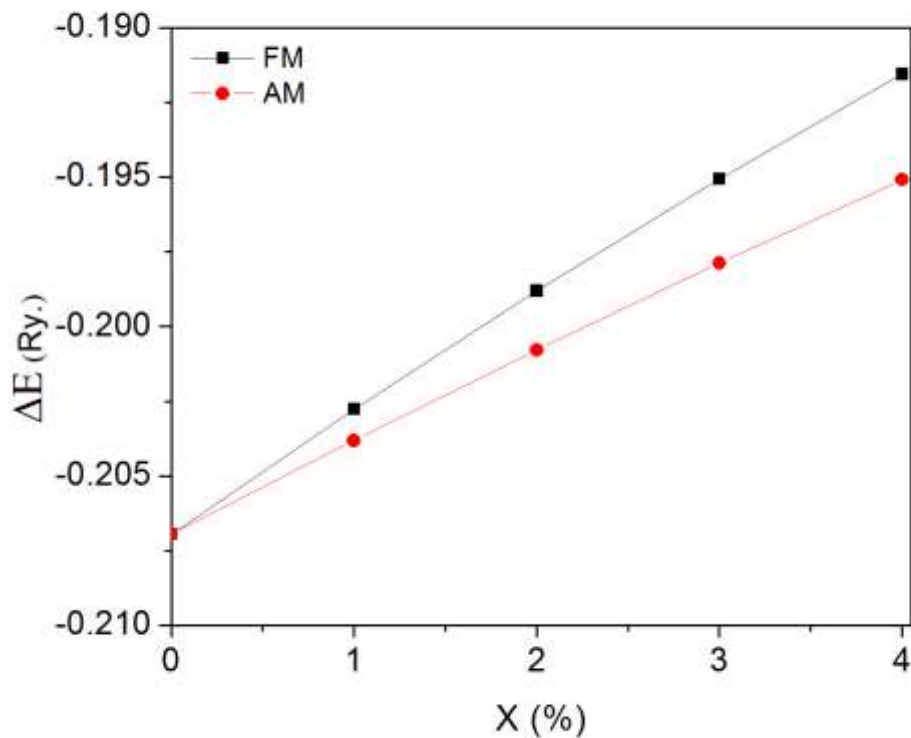


Figure 3.2 Total energy calculations for the $(\text{Mn}_{50-x}\text{Ti}_x)^{1a,1c}(\text{Al}_{46}\text{Mn}_x\text{Ti}_{4-x})^{2e}$ system.

3.2.3. Magnetic experimental investigations of $Mn_{54-x}Al_{46}Ti_x$ ($x = 2; 4$) alloys

The temperature dependences of magnetization measured in low magnetic field $\mu_0H = 0.1$ T for the as-cast and annealed $Mn_{52}Al_{46}Ti_2$ and $Mn_{50}Al_{46}Ti_4$ samples are shown in Figure. 3.7 and Figure.3.8 respectively. The Curie temperature, obtained in molecular field approximations are given in Table 3.5.

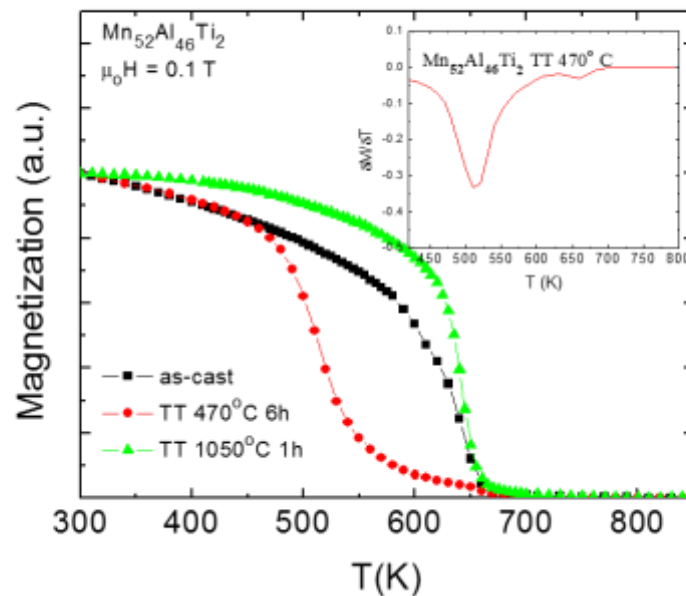


Figure 3.7 The temperature dependence of magnetizations for $Mn_{52}Al_{46}Ti_2$ alloys measured in 0.1 T magnetic field. In the inset is shown the temperature dependence of the differential magnetization for the sample annealed at 470°C for 6h.

The virgin magnetization curve and the demagnetization curves in magnetic field of ± 7 T at 4 K for $Mn_{52}Al_{46}Ti_2$ and $Mn_{50}Al_{46}Ti_4$ alloys are shown in Figure.3.11. and Figure.3.12 respectively. Similar dependences were obtained for these alloys at 300 K. The spontaneous magnetizations values were obtained using the law of approaching to saturation, equation 2.8, coercive field and remanent magnetization are given in the Table 3.5.

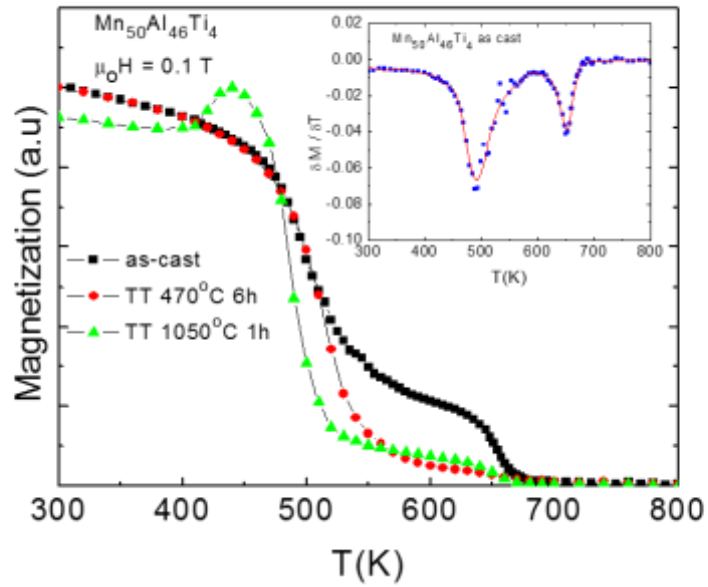


Figure 3.8 The temperature dependence of the magnetizations for the $Mn_{50}Al_{46}Ti_4$ alloys measured in 0.1 T magnetic field. In the inset is shown the temperature dependence of the differential magnetization for the as-cast sample.

Table 3.1 Spontaneous magnetizations, Curie temperatures, coercive fields and remanent magnetizations of $Mn_{52}Al_{46}Ti_2$ and $Mn_{50}Al_{46}Ti_4$ alloys.

Sample	M_s (4K) (Am^2/Kg)	M_s (4K) ($\mu_B/f.u.$)	$M_s(300K)$ (Am^2/Kg)	T_c^T (K)	T_c^K (K)	H_C^{4K} (kOe)	H_C^{300K} (kOe)	M_r^{4K} (Am^2/Kg)	M_r^{300K} (Am^2/Kg)
$Mn_{54}Al_{46}$ [20]TT 470°C 6h	112	0.84	109	645	-	-	0.95	-	21
$Mn_{52}Al_{46}Ti_2$ as-cast	91.20	0.68	93.50	654	-	1.64	0.88	27.48	21.05
$Mn_{52}Al_{46}Ti_2$ TT 470°C 6h	116.00	0.87	87.60	668	534	0.82	0.69	19.51	14.60
$Mn_{52}Al_{46}Ti_2$ TT 1050°C 1h	102.31	0.77	98.54	651	-	0.77	0.54	19.51	17.45
$Mn_{50}Al_{46}Ti_4$ as-cast	80.50	0.60	81.21	664	531	1.13	0.43	15.84	11.02
$Mn_{50}Al_{46}Ti_4$ TT 470°C 6h	99.70	0.75	75.54	668	530	-	0.34	-	11.02
$Mn_{50}Al_{46}Ti_4$ TT 1050°C 1h	90.70	0.68	83.10	664	501	0.76	0.34	16.16	8.52

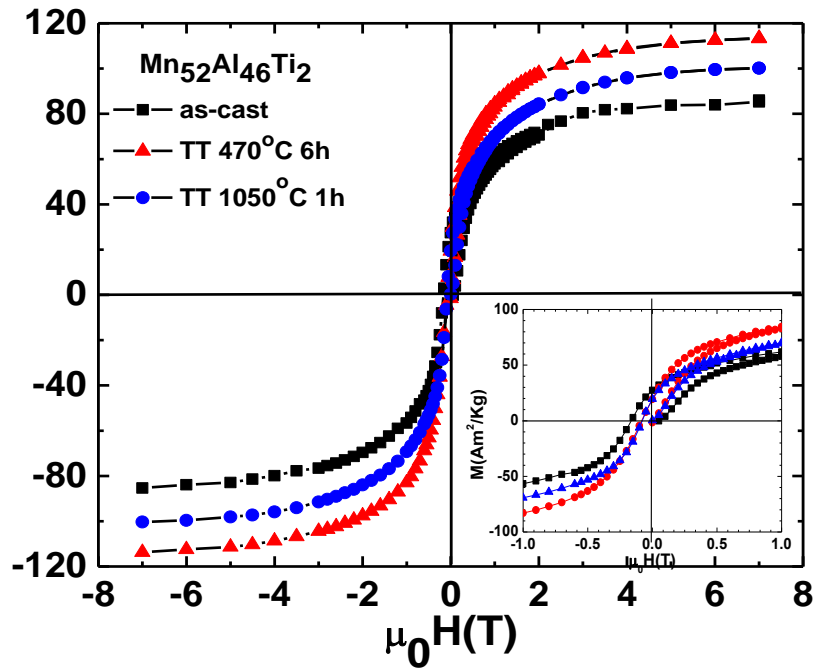


Figure 3. 3 The virgin magnetization curve and the demagnetization curves for the as-cast and annealed $Mn_{52}Al_{46}Ti_2$ samples at 4 K. In the inset is shown the region around the origin of the plot.

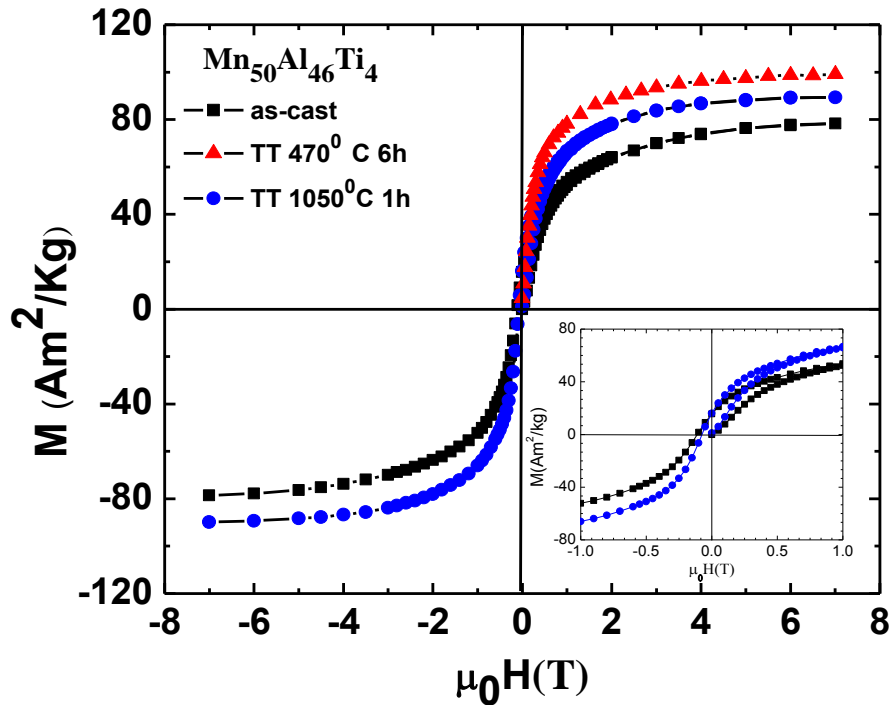


Figure 3. 4 The virgin magnetization curve and the demagnetization curves for the as-cast and annealed $Mn_{50}Al_{46}Ti_4$ samples at 4 K. In the inset is shown the region around the origin of the plot.

3.3 Conclusions

All the analyzed samples contain τ and γ_2 phases. Moreover, $\text{Mn}_{52}\text{Al}_{46}\text{Ti}_2$ alloy annealed at 470 °C for 6 h and $\text{Mn}_{50}\text{Al}_{46}\text{Ti}_4$ alloys include a supplementary κ phase (CsCl- type structure). Band structure calculations show a preference for Ti atoms to occupy the Mn sites in the plane of Al atoms. The increase of the Ti content from $x = 2$ to $x = 4$ in $\text{Mn}_{54-x}\text{Al}_{46}\text{Ti}_x$ leads to the decrease of the τ phase content and consequently to the increase of the soft ferromagnetic κ phase. The best magnetic characteristics were obtained for $\text{Mn}_{52}\text{Al}_{46}\text{Ti}_2$ alloy annealed at 470 °C for 6 h, which are superior to those found in the $\text{Mn}_{54}\text{Al}_{46}$ parent alloy. The values of the Curie temperatures and of the spontaneous magnetizations of the as-cast and annealed $\text{Mn}_{52}\text{Al}_{46}\text{Ti}_2$ and $\text{Mn}_{50}\text{Al}_{46}\text{Ti}_4$ alloys suggest that the solubility limit of Ti in τ -phase of $\text{Mn}_{54-x}\text{Al}_{46}\text{Ti}_x$ is closed to $x=2$ Ti concentration.

Chapter 4.

Structural, Magnetic and Electronic Properties of some Mn-Based Heusler Alloys

4.1 General aspects regarding Heusler alloys

The Full Heusler compounds are ternary intermetallic alloys, which crystallize in the cubic face centered structure with Cu_2MnAl prototype ($L2_1$ structure, space group $Fm\bar{3}m$ (225)), Figure 4.1 [24]. The chemical stoichiometric composition is X_2YZ type, where X and Y are usually two different transition metals and Z is a nonmagnetic element [24]. In these compounds the X, Y and Z atoms occupy the Wyckoff positions $8c$ ($1/4$ $1/4$ $1/4$), $4a$ (0 0 0) and $4b$ ($1/2$ $1/2$ $1/2$) [25]. Full Heusler type structure consists four interpenetrating fcc sublattices, two of which are equally occupied by X element.

Similar to Full Heusler alloys, the Inverse Heusler compounds have also the chemical stoichiometry X_2YZ , but the sequence of the atoms in this structure is X-X-Y-Z. The structure is described by four interpenetrating fcc sublattices, while the prototype structure of Inverse Heusler compounds is CuHg_2Ti with space group $F\bar{4}3m$ (no. 216) (Figure 4.1) [24]. The occupied sites correspond to the Wyckoff positions $4a$ (0 , 0 , 0) and $4d$ ($3/4$, $3/4$, $3/4$) for X, while the Y and the Z atoms are located at $4b$ ($1/2$, $1/2$, $1/2$) and $4c$ ($1/4$, $1/4$, $1/4$), respectively.

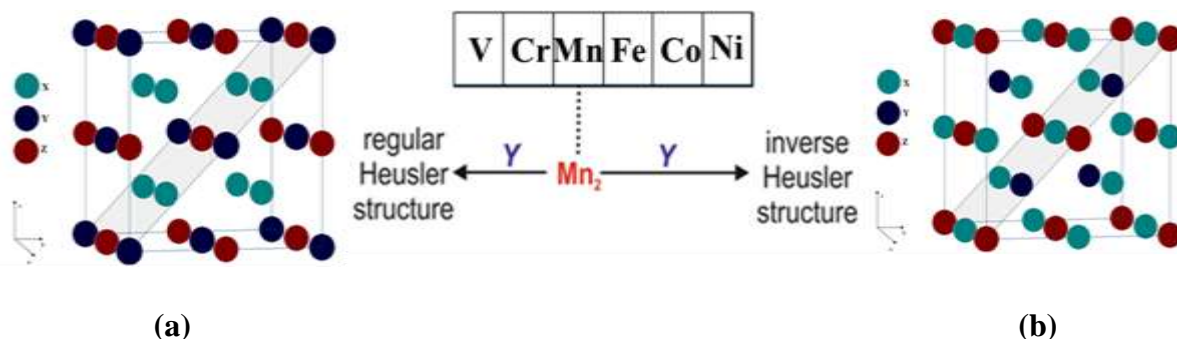


Figure 4.1 X_2YZ $L2_1$ -type crystal structure of Heusler alloys (a) and inverse Heusler (b).

4.2 Influence of the Cu doping on the electronic structure and magnetic properties of the Mn_2VAI Heusler compound [26]

Detailed investigations on the structural, electronic and magnetic properties of the $\text{Mn}_{2-x}\text{Cu}_x\text{VAI}$ ($x = 0, 0.1, 0.2$ and 0.5) Heusler compounds prepared by induction melting have been performed by combined theoretical and experimental approach [26]. The findings of our research provide insight into the evolution of the half-metallic ferrimagnetic material character with disorder and doping. Also, this study demonstrates the restrictions of the Slater – Pauling rule for predicting the half-metallicity of Heusler compounds.

4.2.1. Structural studies of $\text{Mn}_{2-x}\text{Cu}_x\text{VAI}$ alloys ($x = 0, 0.1, 0.2$ and 0.5)

The XRD patterns recorded at room temperature for the as-cast $\text{Mn}_{2-x}\text{Cu}_x\text{VAI}$ alloys ($x = 0, 0.1, 0.2$ and 0.5) are shown in Figure 4.3. In the range of $2\theta = 20$ - 35 degree, the XRD patterns of as-cast and annealed samples are zoomed 6 times on Y scale, in order to evidence the 111 and 200 superstructure peaks. All the XRD peaks correspond to the cubic space group $\text{Fm}\bar{3}\text{m}$ structure (spatial group no. 225) without other detectable impurity phases.

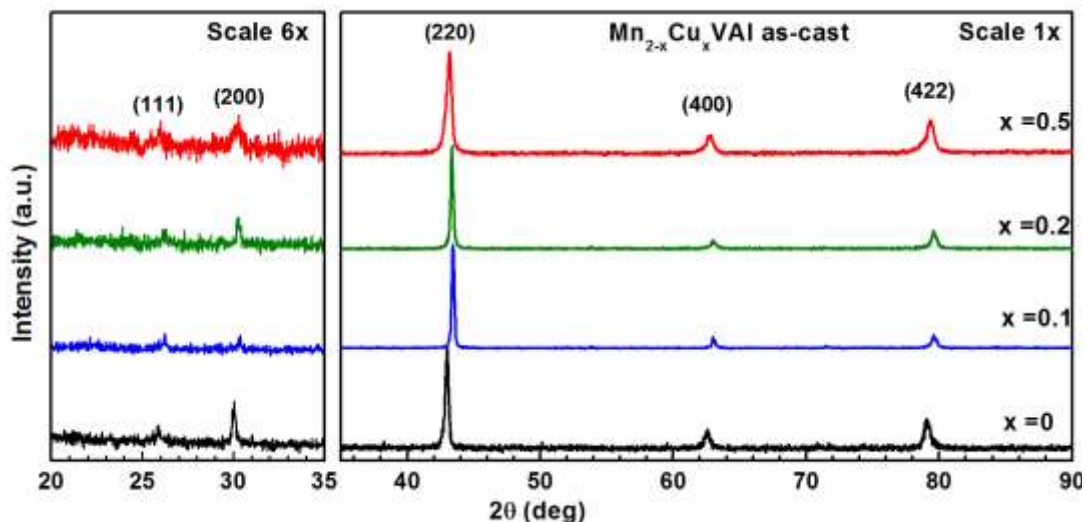


Figure 4.2 X-ray diffraction patterns of the $\text{Mn}_{2-x}\text{Cu}_x\text{VAI}$ as-cast samples. The data are normalized to the intensity of the (220) reflection. XRD patterns are zoomed 6 times on Y scale for 2θ from 20 to 35 deg, left figure.

4.2.2 Band structure calculations in $\text{Mn}_{2-x}\text{Cu}_x\text{VAl}$ alloys ($x = 0, 0.1, 0.2$ and 0.5)

Band structure calculations have been performed using the experimental lattice constants, considering an ideal $L2_1$ structure, without substitutional disorder. The preferential occupation of Cu atoms by doping has been checked by total energy calculations, revealing the preference of Cu atoms for the 8c sites in the crystal structure with cubic space group $Fm\bar{3}m$. The spin resolved densities of states for an 'ideal' and disordered $\text{Mn}_{2-x}\text{Cu}_x\text{VAl}$ system with $L2_1$ structure are shown in Figure. 4.6 a and 4.6 b. As can be seen in this figure, the DOS shows the half-metallic character of the Mn_2VAl , with a gap of ~ 0.2 eV in the spin-up channel at the Fermi level E_F .

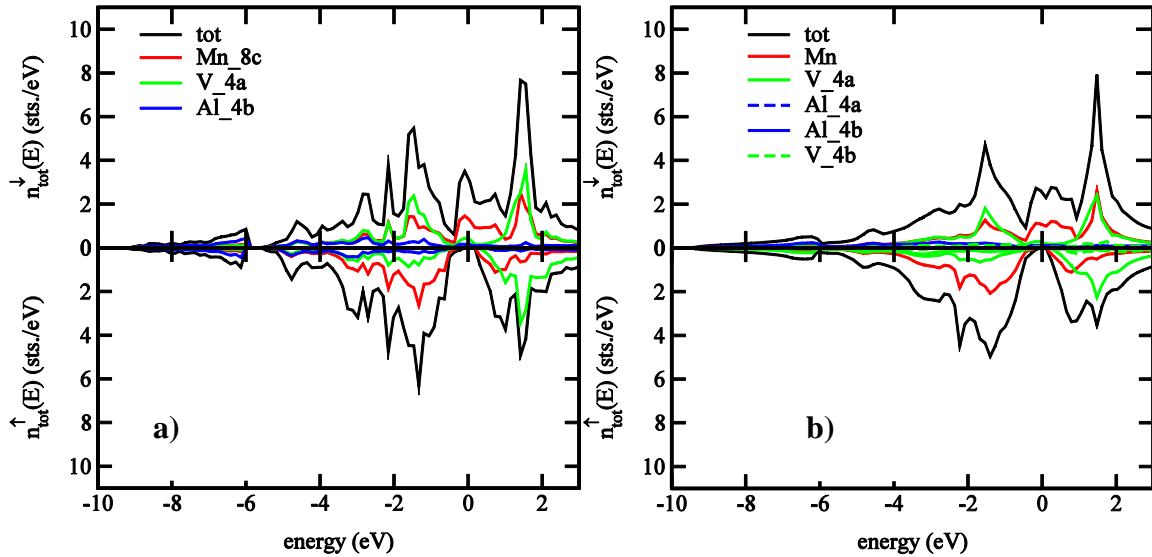


Figure 4.3 The spin-resolved DOS for the 'ideal' (a) and 'disordered' (b) Mn_2VAl . The origin of the energy scale is the Fermi level.

4.2.3 Experimental study of magnetic properties in $\text{Mn}_{2-x}\text{Cu}_x\text{VAl}$ intermetallic compound.

The temperature dependences of the magnetization measured in the low magnetic field for the as-cast and annealed $\text{Mn}_{2-x}\text{Cu}_x\text{VAl}$ samples are shown in Fig. 4.8.

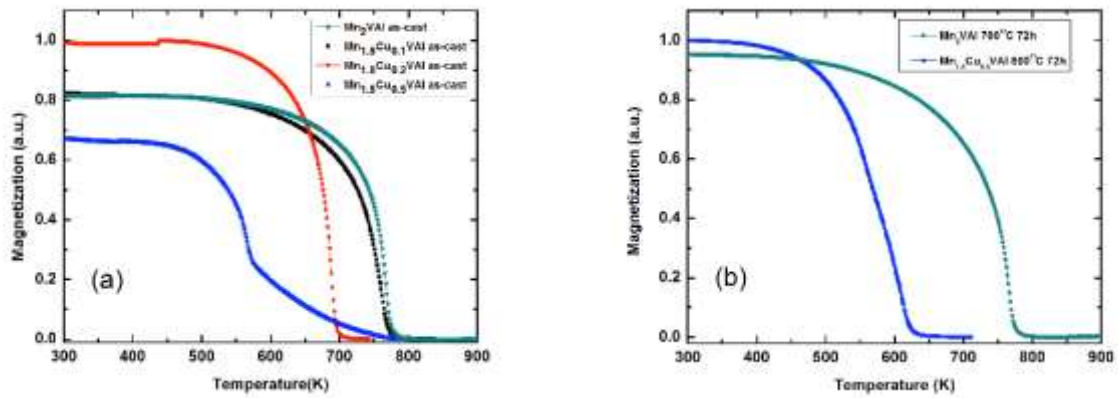


Figure 4.4 The temperature dependence of the magnetization for $Mn_{2-x}Cu_xVAl$ as-cast (a) and annealed alloys (b) measured in low magnetic field.

It was found that the Curie temperatures decrease with the increase of Cu content, ranging between 771 K ($x = 0$) to 580 K ($x = 0.5$) for as-cast samples and 771 K ($x = 0$) to 610 K ($x = 0.5$) for the annealed samples (see Table 4.5).

Table 4.1 The Curie temperatures for $Mn_{2-x}Cu_xVAl$ as-cast and annealed alloys.

Sample	As-cast T_c (K)	Annealed T_c (K)
Mn_2VAl	771	771
$Mn_{1.9}Cu_{0.1}VAl$	763	
$Mn_{1.8}Cu_{0.2}VAl$	692	
$Mn_{1.5}Cu_{0.5}VAl$	580	610

The magnetization curves at 2K, in applied magnetic field up to 10 T, for $Mn_{2-x}Cu_xVAl$ as-cast and annealed samples are presented in Fig.4.9. The spontaneous magnetization values are given in Table 4.6.

Table 4.2 Spontaneous magnetization for $Mn_{2-x}Cu_xVAl$ as-cast and annealed alloys.

Sample	Experiment		Theory	
	As-cast M_s ($\mu_B/f.u.$)	Annealed M_s ($\mu_B/f.u.$)	'disord.' M_s ($\mu_B/f.u.$)	'ideal' M_s ($\mu_B/f.u.$)
Mn_2VAl	1.78	1.78	2.09	2.08
$Mn_{1.9}Cu_{0.1}VAl$	1.72			1.90
$Mn_{1.8}Cu_{0.2}VAl$	1.44			1.74
$Mn_{1.5}Cu_{0.5}VAl$	1.29	1.33	1.14	1.28

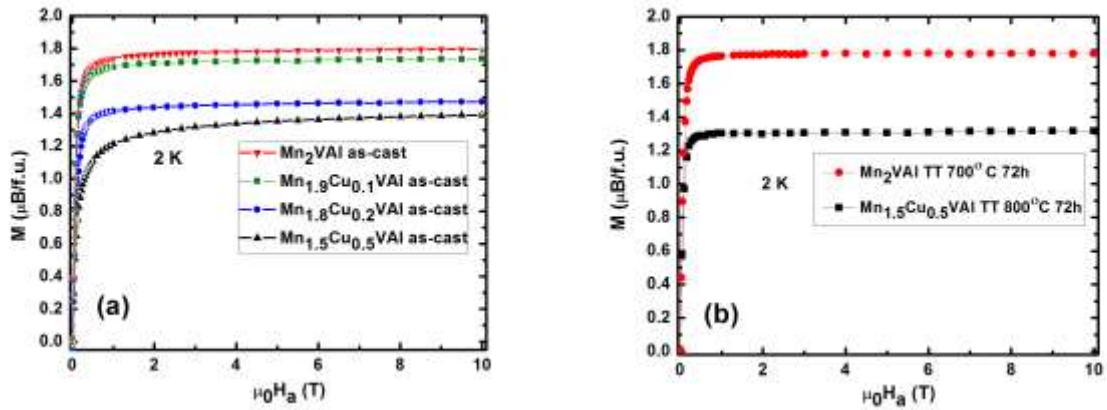


Figure 4.5 Magnetization curves for $Mn_{2-x}Cu_xVAl$ as-cast (a) and annealed (b) alloys measured at 2K.

The obtained values are not in good agreement with Slater-Pauling rule (because the Cu doping leads to the disappearing of the half-metallic character).

4.3. Study of the ferrimagnetism and disorder in the half-metallic $Mn_{2-x}Co_xVAl$ Heusler alloy [28 - 29]

Detailed theoretical and experimental investigations on the structural, electronic and magnetic properties of the $Mn_{2-x}Co_xVAl$ Heusler compounds ($x= 0, 0.2, 0.6, 1$) with $L2_1$ structure are presented.

4.3.1. Structural studies of $Mn_{2-x}Co_xVAl$ Heusler compounds

The $Mn_{2-x}Co_xVAl$ alloys crystallize in a full Heusler ($L2_1$) structure, where the Mn/Co atoms occupy the 8c positions at $(1/4 \ 1/4 \ 1/4)$ and $(3/4 \ 3/4 \ 3/4)$, V occupy the 4a positions at $(0 \ 0 \ 0)$ and Al occupy the 4b positions at $(1/2 \ 1/2 \ 1/2)$ [25] .

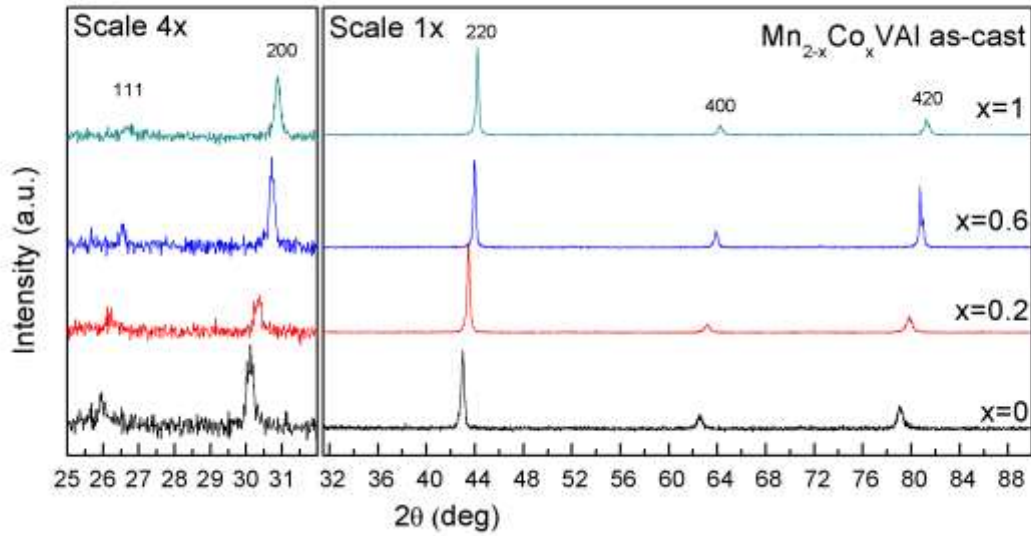


Figure 4.6 Room temperature X-ray diffraction pattern of the as-cast $Mn_{2-x}Co_xVAI$ samples. The data are normalized to the intensity of the (220) reflection. The superstructure peaks are zoomed 6 times on Y scale for 2θ from 25 to 32 deg., left figure.

The XRD patterns at room temperature of the as-cast $Mn_{2-x}Co_xVAI$ ($x = 0, 0.2, 0.6$ and 1) alloys are shown in Figure.4.11. The XRD patterns prove that the as-cast alloys crystallize in a single phase, corresponding to X_2YZ Heusler type structure, cubic space group $Fm\bar{3}m$ (spatial group no. 225), where the Mn and Co atoms occupy the 8c Wyckoff sites (X), while V and Al atoms are placed on the 4a (Y) and 4b (Z) crystal site, respectively.

4.3.2. X-ray photoelectron spectra of $Mn_{2-x}Co_xVAI$ alloys ($x = 0, 0.2, 0.6$ and 1.0)

The Mn $3s$ and V $3s$ core level spectra of the Mn_2VAI alloy show an exchange splitting arising from the exchange interactions between the core hole and the open $3d$ shells. This is a direct evidence of the local magnetic moments on Mn and V sites. The exchange interaction J_{dc} between the core hole spin s and the $3d$ electron spin S gives rise to a satellite on the high binding energies of the main lines of the Mn $3s$ and V $3s$ spectra, respectively. In Figures. 4.16 and 4.17 are shown the curve fitting results of the Mn $3s$ and V $3s$ spectra respectively for Mn_2VAI alloy, after the background subtraction of Shirley type [29].

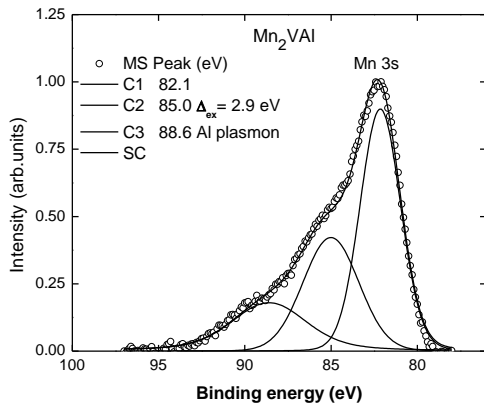


Figure 4.7 XPS spectra of Mn 3s in Mn₂VAI alloy

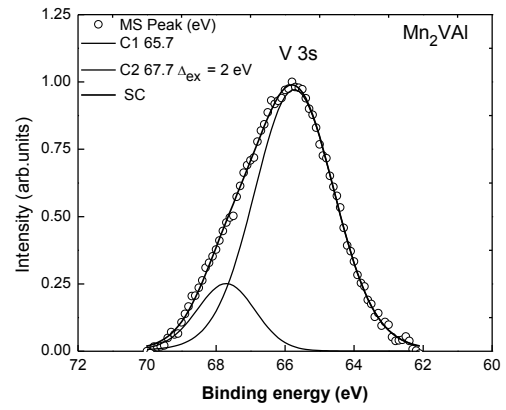


Figure 4.8 XPS spectra of V 3s in Mn₂VAI alloy

4.3.3. Band structure calculations in Mn_{2-x}Co_xVAI alloys (x = 0, 0.2, 0.6 and 1.0)

The calculated magnetic moments of the constituent elements in the Mn_{2-x}Co_xVAI (x = 0, 0.2, 0.6 and 1.0) alloys are given in Table 4.9.

Table 4.3 The calculated magnetic moments of the Mn_{2-x}Co_xVAI alloys.

Mn _{2-x} Co _x VAI		Spin moment	Orbital moment	Slater-Pauling
x = 0 <i>a</i> _{lat} = 5.89 Å		m_s (μB)	m_l (μB)	 m(μB)
	Mn 8c	1.58	0.03	
	V 4a	-1.09	0.01	
	Al 4b	-0.04	0.00	
	Total	2.04	0.07	2.0
x = 0.2 <i>a</i> _{lat} = 5.88 Å	Mn 8c	1.45	0.03	
	Co 8c	-0.22	0.00	
	V 4a	-0.92	0.01	
	Al 4b	-0.03	0.00	
	Total	1.63	0.05	1.6
x = 0.6 <i>a</i> _{lat} = 5.83 Å	Mn 8c	1.07	0.01	
	Co 8c	-0.14	0.00	
	V 4a	-0.59	0.01	
	Al 4b	-0.01	0.00	
	Total	0.81	0.03	0.8
x = 1.0 <i>a</i> _{lat} = 5.80 Å	Mn 8c	0.20	0.00	
	Co 8c	-0.08	0.00	
	V 4a	-0.10	0.00	
	Al 4b	0.00	0.00	
	Total	0.03	0.00	0.0

The experimentally determined lattice constants have been used. An antiferromagnetic coupling between Mn 8c and V 4a spins was found, in agreement with other calculations [31–34].

4.3.4. Magnetic behavior of $\text{Mn}_{2-x}\text{Co}_x\text{VAI}$ Heusler alloys

The isothermal magnetization curves recorded at 2 K and thermo-magnetization curves for $\text{Mn}_{2-x}\text{Co}_x\text{VAI}$ alloys are shown in Figure 4.21 and Figure 4.22, respectively. The values of spontaneous magnetizations, M_s , determined from magnetization isotherms and the Curie temperatures T_c determined in the molecular field approximation from the $M^2(T)$ plot are given in Table 4.10. The spontaneous magnetization decreases upon increasing the Co content, in good agreement with the expectation from the Slater-Pauling rule, due to the increase of the electron numbers through the Co for Mn substitution.

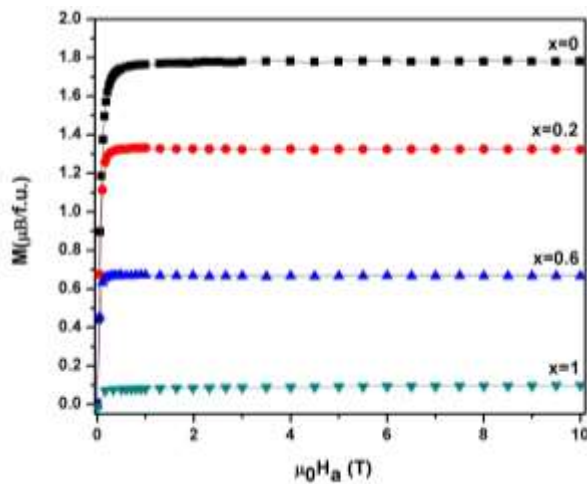


Figure 4.9 Magnetization curves of $\text{Mn}_{2-x}\text{Co}_x\text{VAI}$ alloys at 2K in magnetic field up to 10 T, annealed at 700 °C ($x=0$) and 800 °C ($x=0.2, 0.6$ and 1).

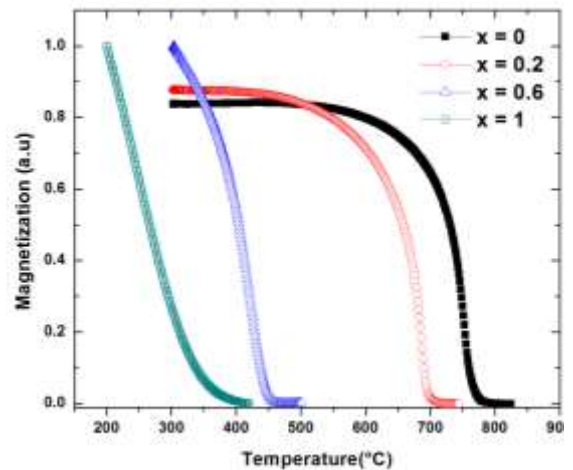


Figure 4.10 Temperature dependences of the magnetization for $\text{Mn}_{2-x}\text{Co}_x\text{VAI}$ alloys annealed at 700 °C ($x=0$) and 800 °C ($x=0.2, 0.6$ and 1) measured in low magnetic fields.

Table 4.4 The spontaneous magnetizations and the Curie temperatures of $Mn_{2-x}Co_xVAl$ alloys determined in this work and from literature data.

Co content (x)	$M_s(\mu_B/f.u)$		$M_s(\mu_B/f.u)$ (Calculated, Table 4.9)	$T_c(K)$	
0	1.78	1.88[34] 1.94[35]	2.04	771	750[34] 760[35]
0.2	1.35		1.63	690	
0.6	0.68		0.81	445	
1.0	0.05	0.07 [34]	0.03	289	105[34]

4.4 Half-metallic compensated ferrimagnetism in the Mn-Co-V-Al Heusler alloys [36]

In these subchapters are detailed theoretical and experimental investigations on the electronic and magnetic properties of the $Mn_2Co_{1-x}V_xAl$ Heusler compounds ($x = 0, 0.1, 0.3$ and 0.5).

4.4.1 Structural characterization of the $Mn_2Co_{1-x}V_xAl$ samples

The XRD data analysis indicates that $Mn_2Co_{1-x}V_xAl$ ($x = 0, 0.1, 0.3$ and 0.5) Heusler alloys are single phases. All the XRD patterns (see figure 4.23) display the superlattice peaks (111) and (200), which is an indication for a highly ordered structure in our as-cast samples, more pronounced for the samples with $x = 0.1$ and 0.5 .

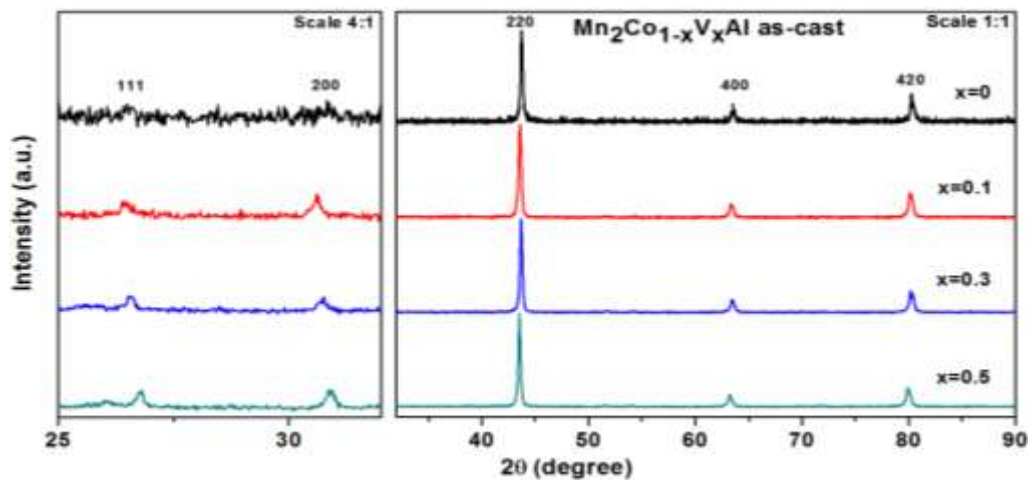


Figure 4.11 The XRD patterns for $Mn_2Co_{1-x}V_xAl$ ($x = 0, 0.1, 0.3$ and 0.5) Heusler alloys.

4.4.2 Band structure calculations in $\text{Mn}_2\text{Co}_{1-x}\text{V}_x\text{Al}$

In the Hg_2CuTi structure type (space group $F\bar{4}3m$, no. 216) of the Mn_2CoAl Heusler alloy the site occupation with the Co $4a$ (0 0 0), Mn $4b$ (1/4 1/4 1/4), Mn $4c$ (1/2 1/2 1/2) and Al $4d$ (3/4 3/4 3/4) atoms has been considered, in agreement with the empirical rule [37]. According to this rule, the atoms with more valence electrons (Co) occupy the $4a$ or $4c$ sites, whilst the Mn atoms occupy neighbor $4b$ and $4c$ sites [36 – 38]. By V for Co substitution on the $4a$ site, due to the V/Co average valence electrons number the Hg_2CuTi structure type is expected to be preserved.

4.4.3 Magnetic behavior of $\text{Mn}_2\text{Co}_{1-x}\text{V}_x\text{Al}$ Heusler alloys.

The magnetic isothermal curves recorded at 2K and thermo-magnetic curves measured in low magnetic field for the $\text{Mn}_2\text{Co}_{1-x}\text{V}_x\text{Al}$ Heusler alloys are shown in Figure. 4.26 and Figure. 4.27, respectively. The Curie temperatures were determined using the molecular field approximation, equation 2.8, from thermomagnetic measurements, Figure 4.27. The values of the spontaneous magnetization and Curie temperatures are summarized in Table 4.13.

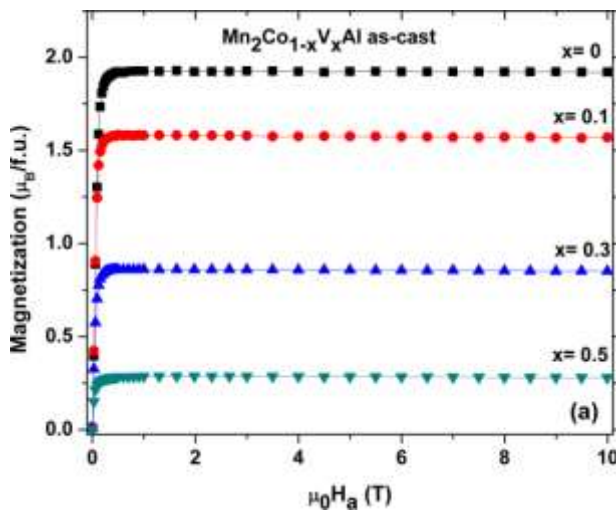


Figure 4.12 Magnetization isotherms at 2 K in a magnetic field up to 10 T for $\text{Mn}_2\text{Co}_{1-x}\text{V}_x\text{Al}$ alloys

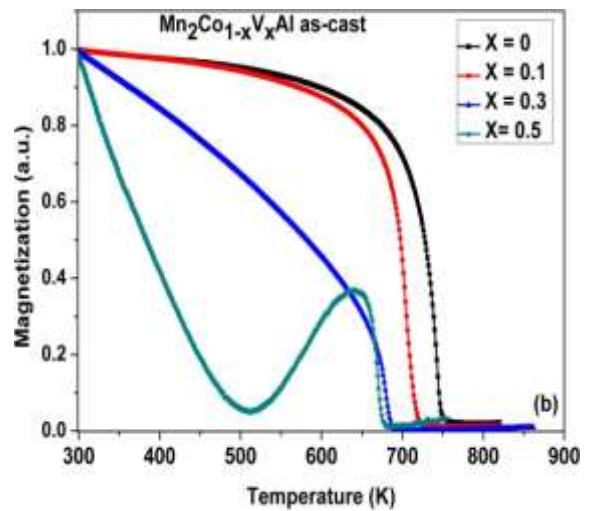


Figure 4.13 Temperature dependence of magnetization for $\text{Mn}_2\text{Co}_{1-x}\text{V}_x\text{Al}$ alloys measured in low magnetic fields.

Table 4.5 The spontaneous magnetization and the Curie temperatures of the $\text{Mn}_2\text{Co}_{1-x}\text{V}_x\text{Al}$ Heusler alloys determined by magnetic measurements and from literature data.

V content (x)	M_s ($\mu\text{B}/\text{f.u.}$)		$T_c(\text{K})$	
0	1.93	2.06 [39]	745	741 [41]
				720 [42]
0.1	1.58		712	
0.3	0.86		699	
0.5	0.29	0.06 [39]	671	659 [41]

4.5 Conclusions

The investigations of the electronic and magnetic properties of the $\text{Mn}_{2-x}\text{Cu}_x\text{VAl}$ alloys ($x = 0, 0.1, 0.2$ and 0.5) reveal the effect of Cu for Mn substitution in these compounds. The Cu doping has an important influence on the magnetic properties of the $\text{Mn}_{2-x}\text{Cu}_x\text{VAl}$ compounds. The reduction of the concentration of the magnetic atoms leads to the decrease of the exchange interactions and subsequently to the overall decrease of the magnetic moments and Curie temperatures. It has been shown that the magnitude of the magnetic moment in the doped X_2YZ type Heusler compounds is strongly influenced by the Y-Z disorder.

The spin-up gap is determined by the crystal field splitting, the local symmetry and coordination of the Mn atoms, which is influenced by the hybridization with Cu atoms. The Cu 3d states are situated at about -3eV under the Fermi level, but their 4s states are situated at Fermi level, hybridizing with the Mn 3d states. As a consequence, the spin-up band gap closes and the half-metallic character of the Mn_2VAl is lost for the Cu ($x = 0.5$) doped compound. The Y-Z disorder effects on the electronic structure shows a broadening of the DOS, which extends under -8 eV. On the other hand, the disappearance of the half-metallic character is shown to be not related to the L_{21} type of disorder evidenced in the XRD patterns for the investigated samples.

Bulk $\text{Mn}_{2-x}\text{Co}_x\text{VAl}$ ($x = 0, 0.2, 0.6$ and 1) alloys have been prepared by induction melting. The crystal structure investigated by XRD and neutron diffraction shows that all the analyzed

samples are single phases belonging to the stable $L2_1$ (spatial group no. 225) structural order. The degrees of $L2_1$ and B2 order parameter have been calculated from the peaks ratios of the XRD patterns using the Takamura's extended order model for Heusler compounds. The annealing of the as-cast samples leads to an improvement of the order parameters, which could be observed also from the reduction of the lattice parameters. The $3s$ core levels of Mn and V determined by XPS show the decrease of the individual spin moments of Mn and V by increasing the Co content in these Heusler alloys. Also, the $3d$ band filling by increasing the Co content was evidenced by XPS.

The band structure calculations show that Mn_2VAl is a half-metal with the total spin moment of $2.04 \mu_B$, having the spin moments of Mn ($1.58 \mu_B$) and V ($-1.09 \mu_B$) ferrimagnetically coupled. By Co doping, the total magnetic moments in the $Mn_{2-x}Co_xVAl$ decrease, being close to zero ($0.03 \mu_B$) in the $MnCoVAl$ Heusler compound, in agreement with the prediction of Galanakis et al. [43] and the weakness of the Co magnetic moment expected from the here reported XPS spectra. The electronic band structure calculations show also that the half-metallic character is preserved for the $Mn_{2-x}Co_xVAl$ with $x = 0, 0.2$ and 0.6 . For $x = 1$, the $MnCoVAl$ compound loses its half-metallic character for the experimental lattice constant (5.80 \AA), but for a narrow range between 5.86 and 5.88 \AA this character can be acquired according to our calculations.

The magnetic behavior show the agreement of the magnetization with the Slater-Pauling rule and a decrease of the Curie temperature with Co content, as was previously reported [34]. A considerably higher value of T_c (289 K) for $MnCoVAl$ ($x = 1$) has been obtained compared with others values reported in literature data those obtained by Deka et al. (105 K) [34]. Low individual spin magnetic moments obtained by band structure calculations and confirmed by photoemission measurements is the main hindrance for the spintronic application of this alloy.

We found significant influence of the preferential site occupation of V on the magnetization of the $Mn_2Co_{1-x}V_xAl$ **Heusler alloys** ($x = 0, 0.1, 0.3$ and 0.5). Theoretical studies show that a fully compensated HMF_i behavior can be obtained for $Mn_{1.92}Co_{0.5}V_{0.58}Al$ and $Mn_{2.07}Co_{0.43}V_{0.5}Al$ alloys. The Curie temperature of the stoichiometric $Mn_2Co_{0.5}V_{0.5}Al$ alloy is 671 K and one expects to be less affected by the off- stoichiometry. As consequence, our theoretical and experimental investigations show evidence for a new Heusler alloy as possible component of a promising class of materials with low power-consumption for spintronic applications.

5. General conclusions

The main objective of this thesis was to study the influence of compositional changes performed by doping in several Mn-based intermetallic alloys on the crystallographic structure, electronic structure, magnetic properties as well as the sign of the interactions between the local magnetic moments. We investigated materials from two different classes: Rare-Earth Free Permanent Magnets (τ -MnAl phase) and Mn-based Full Heusler alloys (Mn_2XY). The detailed conclusions for each studied system have been described in Chapters 3 and 4. Some general outcomes of the presented study are summarized below.

All the analyzed samples were synthesized through induction melting, followed by different annealing procedures. The heat treatments of the as-cast samples lead to several structural changes evidenced in lattice parameter changes, defects and stresses reduction, atomic ordering degree etc. Consequently, magnetic properties of the investigated samples are highly susceptible to annealing parameters. These aspects are well connected with the high sensitivity of the magnetic behavior of the 3d transition elements to the local atomic environment. We observed that these changes are reflected on improved spontaneous magnetization and Curie temperature values in annealed samples compared with the corresponding values for the as-cast samples.

Our investigations in $\text{Mn}_{54-x}\text{Al}_{46}\text{Ti}_x$ alloys followed two main objectives: (i) to promote the formation of the τ magnetic phase and (ii) to decrease the effect of the negative exchange interactions on the total magnetization. Our studies conclude that these goals were partially achieved through controlled Ti for Mn substitution and by appropriate heat treatments.

The magnetic vicinity of Mn magnetic ions and the atomic ordering degree in Mn_2XY Heusler alloys were modified in three modes: (i) by partial substitution of Mn by Cu in $\text{Mn}_{2-x}\text{Cu}_x\text{VAl}$; (ii) by partial substitution of Mn by Co in $\text{Mn}_{2-x}\text{Co}_x\text{VAl}$ and (iii) by balancing the content of Co and V in $\text{Mn}_2\text{Co}_{1-x}\text{V}_x\text{Al}$ alloys. The experimental data and the theoretical calculations showed agreement concerning the influence of Mn magnetic atoms concentration reduction which leads to the decrease of the exchange interactions and subsequently to the overall decrease of the magnetic moments and Curie temperatures. The half metallic behavior in the studied Heusler alloys estimated by band structure calculation is preserved in most of the studied alloys, being in good agreement with experimental findings. The atomic ordering was improved by annealing, being related to the lattice parameters reduction. Increasing the atomic ordering degree has significant influence on the magnetic moments of the studied alloys. Also, by

controlling the Co vs. V ratio in $\text{Mn}_2\text{Co}_{1-x}\text{V}_x\text{Al}$ it was shown that a compensated ferrimagnetic alloy can be obtained.

Publications during the Phd period

1. ISI published articles

1. **R. Gavrea**, R.Hirian, S. Mican, D. Benea, O. Isnard, M. Coldea and V. Pop , "Structural, electronic and magnetic properties of the $Mn_{54-x}Al_{46}Ti_x$ ($x = 2; 4$) alloys", INTERMETALLICS 2017 Volume: 82 Pages: 101-106; IF: 3.35; AIS: 0.67
2. **R. Gavrea**, A. Bolinger, V. Pop, O. Isnard, M. Coldea and D. Benea , "Influence of the Cu doping on the Electronic Structure and Magnetic Properties of the Mn_2VAl Heusler compound", PHYSICA STATUS SOLIDI B-BASIC SOLID STATE PHYSICS 2017 Volume: 254 Pages:1-7 IF: 1.45; AIS: 0.5
3. **R. Gavrea**, C. Leostean, M. Coldea, O Isnard, V. Pop and D. Benea, "Effect of Co for Mn substitution on the electronic properties of $Mn_{2-x}Co_xVAl$ as probed by XPS", INTERMETALLICS 2018 Volume: 93 Pages: 155-161; IF: 3.35; AIS: 0.67
4. **R. Gavrea**; M. Coldea; L. Barbu-Tudoran; O. Isnard; V. Pop; D. Benea, "Reduction of the substitutional disorder by heat treatments in $Mn_{2-x}Co_xVAl$ Heusler alloys", POWDER METALLURGY AND ADVANCED MATERIALS, 2018, Volume: 8 Pages: 219-227
5. D. Benea, **R. Gavrea**, M. Coldea, O Isnard, V. Pop, " Half-metallic compensated ferrimagnetism in the Mn-Co-V-Al Heusler alloys", Journal of Magnetism and Magnetic Materials, 2019 Volume 475, Pages 229-233 IF: 2.68; AIS: 0.5

2. Conferences and Summer Schools

1. **Poster: R. Gavrea, T. Radu, V. Pop, O. Isnard, D. Benea International Summer School of Physical and Chemical Principles in Materials Science 2016 July 11-17, 2016 in Paris – France, “STRUCTURAL, MAGNETIC AND ELECTRONIC PROPERTIES OF $Mn_{2-x}Co_xVAl$ ($X=0, 0.2, 0.6, 1$) HEUSLER ALLOYS”**
2. **Poster: R. Gavrea, R.Hirian, S. Mican, D. Benea, O. Isnard, M. Coldea and V. Pop, 24th International Workshop on Rare-Earth and Future Permanent Magnets and Their Applications (REPM 16) 28 August to 1 September 2016 Darmstadt, Germany, “Structural, electronic and magnetic properties of the $Mn_{54-x}Al_{46}Ti_x$ ($x = 2; 4$) alloys”**
3. **Poster: R. Gavrea, D. Benea, R. Hirian, T. Radu, R. Erhan, M. Coldea and V. Pop 11th International Conference On Physics Of Advanced Materials (ICPAM-11), 8th to 14th of September, 2016 Cluj-Napoca, Romania, “THE INFLUENCE OF THE CO DOPING ON THE ELECTRONIC AND MAGNETIC PROPERTIES OF THE HALF-METALLIC FERRIMAGNET Mn_2VAl ”**
4. **Oral: R. Gavrea, D. Benea, T. Radu, R. Erhan and V. Pop Presentation: 16th International Balkan Workshop on Applied Physics and Materials Science IBWAP 2016 (7-9, July, 2016) Constanta, Romania, “INVESTIGATIONS OF THE FERRIMAGNETISM AND DISORDER IN THE HALF-METALLIC HEUSLER ALLOY $Mn_{2-x}Co_xVAl$ “**
5. **Poster: R. Gavrea, A. Bolinger, V. Pop, O. Isnard and D. Benea, TIM 17 Physics Conference 2017 May 25-27, 2016 in Timisoara – Romania, “Influence of the Cu doping on the Electronic Structure and Magnetic Properties of the Mn_2VAl Heusler compound”**
6. **Poster: R. Gavrea, A. Bolinger, V. Pop, O. Isnard and D. Benea, The European Conference PHYSICS OF MAGNETISM 2017 (PM'17) June 26-30, 2017 Poznań, POLAND, “Influence of the Cu doping on the Electronic Structure and Magnetic Properties of the Mn_2VAl Heusler compound”**
7. **Poster: R. Gavrea, A. Bolinger, V. Pop, O. Isnard and D. Benea, 11th International Conference Processes in Isotopes and Molecules, 27th to 29th of September, 2017 Cluj-Napoca, Romania, “Influence of the Cu doping on the Electronic Structure and Magnetic Properties of the Mn_2VAl Heusler compound”**
8. **Poster: R. Gavrea, D. Benea, R. Hirian, O. Isnard and V. Pop, 12th International Conference Processes in Isotopes and Molecules, 25th to 27th of September, 2019 Cluj-Napoca, Romania, “Investigations on compensated ferrimagnetism in the $Mn_2Co_{0.5}V_{0.5}Al$ Heusler alloy”**

Partial References:

- [1] Kittel, C. "Introduction to solid state physics". Fifth edition. United Kingdom, 1976.
- [2] Y. Takamura, R. Nakane, and S. Sugahara, "Analysis of L21-ordering in full-Heusler Co₂FeSi alloy thin films formed by rapid thermal annealing," *J. Appl. Phys.*, vol. 105, no. 7, p. 07B109, Mar. 2009.
- [3] J. Baruchel, J.-L. Hodeau, M. S. Lehmann, J.-R. Regnard, and C. Schlenker, Eds., *Neutron and Synchrotron Radiation for Condensed Matter Studies: Applications to Solid State Physics and Chemistry*. Berlin Heidelberg: Springer-Verlag, 1994.
- [4] W. J. O.-T., "Neutron diffraction", (third edition), G.E. Bacon, Clarendon Press, Oxford, 1975, *J. Mol. Struct.*, vol. 33, pp. 344–344, Aug. 1976.
- [5] V. Pop, I. Chicinas, and N. Jumate. "Fizica Materialelor - Metode Experimentale". Presa Universitara Clujeana, Cluj-Napoca, 2001.
- [6] A. Barlet, J. Genna, and P. Lethuillier, "Insert for Regulating Temperatures Between 2-K and 1000-K in a Liquid-Helium Dewar - Description and Cryogenic Analysis" *Cryogenics*, vol. 31, no. 9, pp. 801–805, Sep. 1991.
- [7] "SPRKKR." [Online]. Available: http://ebert.cup.uni-muenchen.de/index.php?option=com_content&view=article&id=8&catid=4&Itemid=7.
- [8] P. Weinberger, "Electron Scattering Theory for Order and Disordered Matter, University Press, Oxford, 1990."
- [9] A. Gonis, "Green Function for Ordered and Disordered Systems", North-Holland, Amsterdam, 1992.
- [10] P. Strange, "Relativistic Quantum Mechanics", University Press, Cambridge, 1998.
- [11] R. Skomski, P. Manchanda, P. K. Kumar, B. Balamurugan, A. Kashyap, and D. J. Sellmyer, "Predicting the future of permanent-magnet materials" *IEEE Trans. Magn.*, vol. 49, no. 7, pp. 3215–3220, 2013.
- [12] N. Poudyal and J. P. Liu, "Advances in nanostructured permanent magnets research" *J. Phys. Appl. Phys.*, vol. 46, no. 4, p. 043001, 2013.
- [13] R. Stamps, S. Breitreutz, J. Åkerman, A. Chumak, Y.C. Otani, G. Bauer, J. Thiele, M. Bowen, S. Majetich, M. Klaui, I. L. Prejbeanu, B. Dieny, N. Dempsey and B. Hillebrands, "The 2014 Magnetism Roadmap" *J. Phys. Appl. Phys.*, vol. 47, no. 33, p. 333001, 2014.
- [14] J. M. D. Coey, "Permanent magnets: Plugging the gap" *Scr. Mater.*, vol. 67, no. 6, pp. 524–529, Sep. 2012.
- [15] P. Manchanda, A. Kashyap, J. E. Shield, L. H. Lewis, and R. Skomski, "Magnetic properties of Fe-doped MnAl," *J. Magn. Magn. Mater.*, vol. 365, pp. 88–92, Sep. 2014.
- [16] A. J. J. Koch, P. Hokkeling, M. G. v. d. Steeg, and K. J. de Vos, "New Material for Permanent Magnets on a Base of Mn and Al," *J. Appl. Phys.*, vol. 31, no. 5, pp. S75–S77, May 1960.

- [17] J. M. D. Coey, “Hard Magnetic Materials: A Perspective,” *IEEE Trans. Magn.*, vol. 47, no. 12, pp. 4671–4681, Dec. 2011.
- [18] R. Skomski and J. M. D. Coey, *Permanent magnetism*. Bristol, UK; Philadelphia, PA: Institute of Physics Pub, 1999.
- [19] R. Gavrea, R. Hirian, S. Mican, D. Benea, O. Isnard, M. Coldea and V. Pop, “Structural, electronic and magnetic properties of the Mn_{54-x}Al₄₆Ti_x (x = 2; 4) alloys” *Intermetallics*, vol. 82, pp. 101–106, Mar. 2017.
- [20] S. Mican, D. Benea, R. Hirian, R. Gavrea, O. Isnard, V. Pop and M. Coldea “Structural, electronic and magnetic properties of the Mn₅₀Al₄₆Ni₄ alloy” *J. Magn. Magn. Mater.*, vol. 401, pp. 841–847, Mar. 2016.
- [21] H. Kōno, “On the Ferromagnetic Phase in Manganese-Aluminum System,” *J. Phys. Soc. Jpn.*, vol. 13, no. 12, pp. 1444–1451, Dec. 1958.
- [22] O. Moze, L. Pareti, and A. E. Ermakov, “Neutron diffraction and magnetic investigations of Ga substituted MnAl permanent magnet materials” *J. Appl. Phys.*, vol. 63, no. 9, pp. 4616–4619, May 1988.
- [23] J. H. Park, Y. K. Hong, S. Bae, J. J. Lee, J. Jalli, G. S. Abo, N. Neveu, S. G. Kim, C. J. Choi, and J. G. Lee, “Saturation magnetization and crystalline anisotropy calculations for MnAl permanent magnet” *J. Appl. Phys.*, vol. 107, no. 9, p. 09A731, Apr. 2010.
- [24] T. Graf, C. Felser, and S. S. P. Parkin, “Simple rules for the understanding of Heusler compounds” *Prog. Solid State Chem.*, vol. 39, no. 1, pp. 1–50, May 2011.
- [25] C. Felser and A. Hirohata, Eds., *Heusler Alloys: Properties, Growth, Applications*. Springer International Publishing, 2016.
- [26] R. Gavrea, A. Bolinger, V. Pop, O. Isnard, M. Coldea, and D. Benea, “Influence of Cu Doping on the Electronic Structure and Magnetic Properties of the Mn₂VAl Heusler Compound” *Phys. Status Solidi B-Basic Solid State Phys.*, vol. 254, no. 11, p. 1700160, Nov. 2017.
- [27] R. Gavrea, M. Coldea, L. Barbu-Tudoran, O. Isnard, V. Pop, and D. Benea, “Reduction of the substitutional disorder by heat treatments in Mn_{2-x}Co_xVAl Heusler alloys” in *Powder Metallurgy and Advanced Materials*, vol. 8, T. F. Marinca, B. V. Neamtu, and F. Popa, Eds. Millersville: Materials Research Forum Llc, 2018, pp. 219–227.
- [28] R. Gavrea, C. Leostean, M. Coldea, O. Isnard, V. Pop, and D. Benea, “Effects of Co for Mn substitution on the electronic properties of Mn_{2-x}Co_xVAl as probed by XPS” *Intermetallics*, vol. 93, pp. 155–161, Feb. 2018.
- [29] R. Hesse, T. Chassé, and R. Szargan, “Peak shape analysis of core level photoelectron spectra using UNIFIT for WINDOWS” *Fresenius J. Anal. Chem.*, vol. 365, no. 1, pp. 48–54, Sep. 1999.
- [30] I. Galanakis, K. Ozdogan, E. Sasioglu, and B. Aktas, “Ab-initio design of half-metallic fully-compensated ferrimagnets: the case of Cr₂MnZ (Z= P, As, Sb, Bi) compounds” *Phys. Rev. B*, vol. 75, no. 17, May 2007.

- [31] I. Galanakis and P. Mavropoulos, “Spin-polarization and electronic properties of half-metallic Heusler alloys calculated from first principles” *J. Phys. Condens. Matter*, vol. 19, no. 31, p. 315213, 2007.
- [32] R. Weht and W. E. Pickett, “Half-metallic ferrimagnetism in Mn_2VAl ” *Phys. Rev. B*, vol. 60, no. 18, pp. 13006–13010, Nov. 1999.
- [33] M. Meinert, J.-M. Schmalhorst, G. Reiss, and E. Arenholz, “Ferrimagnetism and disorder of epitaxial $Mn_{2-x}Co_xVAl$ Heusler compound thin films” *J. Phys. Appl. Phys.*, vol. 44, no. 21, p. 215003, 2011.
- [34] B. Deka, A. Srinivasan, R. K. Singh, B. S. D. C. S. Varaprasad, Y. K. Takahashi, and K. Hono, “Effect of Co substitution for Mn on spin polarization and magnetic properties of ferrimagnetic Mn_2VAl ” *J. Alloys Compd.*, vol. Complete, no. 662, pp. 510–515, 2016.
- [35] C. Jiang, M. Venkatesan, and J. M. D. Coey, “Transport and magnetic properties of Mn_2VAl : Search for half-metallicity” *Solid State Commun.*, vol. 118, pp. 513–516, Jun. 2001.
- [36] D. Benea, R. Gavrea, M. Coldea, O. Isnard, and V. Pop, “Half-metallic compensated ferrimagnetism in the Mn-Co-V-Al Heusler alloys” *J. Magn. Magn. Mater.*, vol. 475, pp. 229–233, Apr. 2019.
- [37] J. C. Slater, “The Ferromagnetism of Nickel. II. Temperature Effects” *Phys. Rev.*, vol. 49, no. 12, pp. 931–937, Jun. 1936.
- [38] M. Meinert, J.-M. Schmalhorst, and G. Reiss, “Exchange interactions and Curie temperatures of Mn_2CoZ compounds” *J. Phys. Condens. Matter*, vol. 23, no. 11, p. 116005, Mar. 2011.
- [39] G. D. Liu X. F. Dai, H. Y. Liu, J. L. Chen, Y. X. Li, Gang Xiao and G. H. Wu. “ Mn_2CoZ ($Z = Al, Ga, In, Si, Ge, Sn, Sb$) compounds: Structural, electronic, and magnetic properties” *Phys. Rev. B*, vol. 77, no. 1, Jan. 2008.
- [40] Y. J. Zhang, and G. J. Li, E. K. Liu, J. L. Chen, W. H. Wang and G. H. Wu, “Ferromagnetic structures in Mn_2CoGa and Mn_2CoAl doped by Co, Cu, V, and Ti” *J Appl Phys* 113 2013 123901.
- [41] P. V. Midhunlal, J. A. Chelvane, U. M. A. Krishnan, D. Prabhu, R. Gopalan, and N. H. Kumar, “Near total magnetic moment compensation with high Curie temperature in $Mn_2V_{0.5}Co_{0.5}Z$ ($Z = Ga, Al$) Heusler alloys” *J. Phys. Appl. Phys.*, vol. 51, no. 7, p. 075002, 2018.
- [42] S. Ouardi, G. H. Fecher, B. Balke, A. Beleanu, X. Kozina, G. Stryganyuk, and C. Felser, “Electronic and crystallographic structure, hard x-ray photoemission, and mechanical and transport properties of the half-metallic Heusler compound Co_2MnGe ” *Phys. Rev. B*, vol. 84, no. 15, p. 155122, Oct. 2011.
- [43] I. Galanakis, K. Ozdogan, E. Sasioglu, and B. Aktas, “Ab-initio design of half-metallic fully-compensated ferrimagnets: the case of Cr_2MnZ ($Z = P, As, Sb, Bi$) compounds,” *Phys. Rev. B*, vol. 75, no. 17, May 2007.